EASI SMR

D7.1 Specifications of PRATIC fresh core at BOC conditions

Géraud PRULHIÈRE, Aimeric EUSTACHE, Barbara Vezzoni (CEA),
Enrico GIRARDI, Marco TIBERGA (EDF),
Marc-Antoine DOR (FRAMATOME)

1. Document information

Grant Agreement Number	n°101164810
Project Title	Ensuring Assessment of Safety Innovations for SMR
Project Acronym	EASI-SMR
Project Coordinator	Nicolas Sobecki
Project Duration	1 September 2024 – 31 August 2028 (48 months)
Related Work Package	WP7 Advanced Core Physics Studies of Boron-Free SMR-cores
Lead Organisation	CEA
Contributing Partner(s)	EDF, FRAMATOME, ASNR
Submission Date	28/02/2025
Dissemination Level	Public

2. History

Date	Submitted by	Reviewed by	Version (Notes)
28/01/2025	Géraud Prulhière (CEA)	Victor-Hugo Sanchez-Espinoza (KIT)	V0.1
12/02/2025	Victor-Hugo Sanchez-Espinoza (KIT)	Nicolas Sobecki (EDF)	V1
25/02/2025	Géraud Prulhière (CEA)	Nicolas Sobecki (EDF)	V2 submitted

Co-funded by the European Union
UK Research and Innovation
The Research Council of Norway
Project funded by

Table of contents

List of Figures

List of Tables

Co-funded by the European Union
UK Research and Innovation
The Research Council of Norway
Project funded by

3. Summary

One part of the current nuclear reactor research focuses on light water small modular reactors (LW-SMRs), with particular attention on soluble-boron-free (SBF) configurations. SBF designs rely on control rods insertion or extraction movements and burnable neutron poisons (i.e., gadolinium) to regulate reactivity. Additionally, small modular reactors (SMRs) often use steel reflectors to reduce neutron leakage. The compact design of SMRs, combined with these technical solutions, leads to significant fluctuations in neutron flux within the core during normal operational cycles. Therefore, in-depth analysis is crucial, especially regarding reactor performance under both normal and accident conditions, as well as the reliability of neutronics and thermal-hydraulic calculation assumptions. Research into these challenges requires reactor core neutronics benchmarks that align with industrial concepts, ensuring that the analysis results are applicable to real reactors expected to be built in the 2030s.

In this context, Work Package (WP) 7 of the European EASI-SMR project is dedicated to Advanced Core Physics Studies of Boron-Free SMR-cores. This WP focuses on benchmarking activities related to multiphysics simulations for two reactor concepts: a heat-generating reactor named LDR-50-lite, and a power reactor called PRATIC. The object of this deliverable is to describe the technological data of the PRATIC core, to provide the EASI-SMR project partners with all the input data needed to carry out simulations.

The PRATIC benchmark specification consists of two components:

- A "start-up" core made entirely of fresh fuel assemblies;
- An "equilibrium" core, which is composed of half fresh fuel assemblies and half fuel assemblies that have undergone one cycle of irradiation.

The term 'equilibrium cycle' is not really appropriate for this benchmark. It is in fact an assembly loading pattern within the core that is identical for all cycles from number 2 onwards. What distinguishes the start-up core from the equilibrium core is the assembly loading patterns within the core, as described in section 8.3.4.3. On the other hand, the assemblies reloading pattern from one cycle to the next is always the same for each inter-cycle and is described in section 8.6.3, figure 25.

Detailed data for both components is provided in this document and is also available in a GIT repository. Future updates and refinements to the benchmark specification will be made publicly accessible there. Access to this repository can be requested via email at pratic@cea.fr.

4. Keywords

Soluble-boron-free core; input data; light water reactor; neutronics; PRATIC

Co-funded by the European Union
UK Research and Innovation
The Research Council of Norway
Project funded by

5.Abbreviations and acronyms

Acronym	Description
AIC or AgInCd	Alloy of silver, indium and cadmium
AISI 304	See "SS-304"
ARO	All (control) Rods Out
BOC	Beginning of Cycle
BOL	Beginning of Life (means burn-up = 0 MWd/t)
CRI	Critical Rods Insertion
EASI-SMR	Ensuring Assessment of Safety Innovations for SMR
EFPD	Equivalent Full Power Day
ENU	Enriched Natural Uranium
EPR	Evolutionary Power Reactor
EOC	End Of Cycle
FA	Fuel Assembly
LEU	Low-Enriched Uranium
LW-SMR	Light Water Small Modular Reactor
NP	Nominal Power
PRATIC	*"Petit REP Académique pour Tester, Innover & Concevoir"* Small Academic PWR for Test, Innovation & Design
PWR	Pressurized Water Reactor
RCCA	Rod Cluster Control Assembly
SBF	Soluble Boron Free
SMR	Small Modular Reactor
SS-304	Stainless Steel 304 (a grade of austenitic stainless steel)
WP	Work Package
%wt.	The weight ratio (in %)
Zy4	Zircaloy-4

Co-funded by the European Union
UK Research and Innovation
The Research Council of Norway
Project funded by

6. Introduction

In response to global warming, the search for clean, efficient, and reliable energy sources continues to advance, driven by the need for decarbonization and energy security. Nuclear power, with its low carbon footprint and consistent electricity generation, is seen as a potential key player in the future energy mix. In this context, small modular reactors (SMRs) are gaining increasing attention worldwide. These reactors, being smaller than traditional pressurized water reactors (PWRs), offer potential advantages, including streamlined construction, easier deployment, lower construction costs, and standardization in dedicated facilities.

Numerous industrial SMR designs are currently under development across the globe. Among these, some projects focus on the development of soluble-boron-free (SBF) PWR cores. SBF reactor cores are typically chosen to avoid the complications associated with using soluble boron, such as corrosion of structural materials, large volumes of liquid radioactive waste, potential boron dilution accidents, degradation of the moderator temperature coefficient, and the need for boron control and water purification systems. As a result, removing soluble boron from the primary coolant system provides several benefits by simplifying reactor operation and maintenance.

Currently, one method to compensate for excess reactivity in SBF reactor cores is the use of burnable absorbers (such as gadolinium-poisoned fuel rods) and control rods. However, despite the advantages of SBF operation, its reliance on control rods leads to significant variations in power distribution during the irradiation cycle, both axially and radially. Additionally, the widespread use of poisoned fuel rods results in an uneven distribution of burnable poisons within the core, making it more challenging to achieve a uniform radial power distribution compared to larger PWR cores that use soluble boron. These challenges are further amplified in SMRs due to their smaller size and the common use of heavy reflectors (mainly made of steel) to extend the cycle length and flatten the power distribution. As a result, the behaviour of SMR cores may differ significantly from that of larger PWRs, necessitating a detailed examination of the assumptions used in neutronics and thermal-hydraulics calculation schemes.

The potential future use of SBF-PWR type SMRs raises several questions that require further analysis in various research fields. These include studies on reactor behavior during normal operation, transient conditions (both incidental and accidental), potential fuel cycle management scenarios, and sensitivity studies on the application of technological solutions. To address these challenges, scientific research must be aligned with reactor core benchmarks that reflect current industrial developments. This alignment must consider technological choices and performance criteria to ensure that study results are directly applicable to reactors set for deployment.

To meet these needs, the PRATIC project was developed at the French Atomic Energy and Alternative Energy Commission (CEA). PRATIC, which stands for "Petit REP Académique pour Tester, Innover & Concevoir" (Small Academic PWR for Testing, Innovation, and Design), is a SBF-PWR type SMR core benchmark designed for scientific research. It aims to replicate the characteristics of industrial-grade SMR cores, including power output and equilibrium cycle length. The technological solutions employed in PRATIC, such as fuel type, burnable absorbers, control rods, and reflectors, are consistent with those found in established industrial concepts.

EASI-SMR is a project co-funded by the European Union, the UK Research and Innovation government agency, the Research Council of Norway, and the Swiss Secretariat for Education, Research and Innovation. It stands for “Ensuring Assessment of Safety Innovation for SMR”, and it aims at powering a safer future for light-water SMRs. It is composed of 9 work packages (WP),

whose WP7 is dedicated to advanced core physics studies of boron-free SMR-cores. The WP7 aims at providing a comprehensive characterization of boron-free cores and support the safety assessment of SMR cores with validated methods and industrial tools for the analysis of LW-SMR cores. Two boron-free cores will be studied: the PRACTIC and LDR-50-lite, developed by CEA and VTT, respectively.

This document focuses on the PRATIC core. In particular, the document is divided in two main parts:

- An "Overview" section, which gives the guidelines and the assumptions used to design the PRATIC cores, as well as the revision notes. It explains that two cores have been designed: a start-up core composed entirely of fresh fuel assemblies, and an equilibrium core containing half fresh assemblies and half assemblies that have been irradiated during a cycle.
- A "specification" section, which defines in detail the nuclear data to be used, the material compositions, the geometries, the thermal and thermal-hydraulics assumptions and boundary conditions, the reactor management and control strategy, and finally ends with some fuel assemblies and core features.

The appendix details the basic cold (20°C) data used to define the hot data.

Additionally, a GIT repository containing data files for core modelling and various results data (including core k_{eff} in different configurations, burnup distributions, power distributions, etc.) is available for both start-up and equilibrium-cycle cores. This repository will be regularly updated as the PRATIC database expands. Access to the repository can be requested via email at: pratic@cea.fr. The data shared in this document and the GIT repository are licensed under Creative Commons BY-NC-SA 4.0 (BY-NC-SA-4.0 licence deed, 2024), which allows for non-commercial reuse with proper attribution to the authors. The original document to cite for authors attribution is (Vuiart, Eustache, Eveillard, & Prulhière, 2024).

Citation of the original document on the PRATIC core (Available online in open access at: https://www.epj-n.org):

Romain Vuiart, Aimeric Eustache, Sarah Eveillard, Geraud Prulhiere. PRATIC: A soluble-boron-free, pressurized water cooled, SMR core benchmark, EPJ Nuclear Sci. Technol. 10, 25 (2024). https://doi.org/10.1051/epjn/2024026.

7.Overview

This section describes the main assumptions used for the design of the PRATIC core.

7.1. Design guidelines and prior assumptions

7.1.1. Main objectives to design PRATIC core

The design of the PRATIC core began at CEA at the end of 2022, within a team of researchers specialized in neutronics and core design. The objective was to create a virtual core of a light water SMR that can be used for:

- Testing calculation models;
- Conducting some academic research on LW-SMR and communicating the results of that research;
- Developing scientific collaborations.

7.1.2. Assumptions

To be consistent with some up-to-date industrial designs of LW-SMRs (e.g., BWRX-300, CAREM, iSMR, PWR-20, RITM-200, STAR, Rolls-Royce SMR, (Small Modular Reactor Technology Catalogue, 2024)), the designers of PRATIC made the choice of controlling the core reactivity without the help of soluble boron in the moderator of the primary loop. Thus, the reactivity is controlled by:

- A passive system that consists in homogeneously mixing gadolinium oxide poison Gd_2O_3 with UO_2 in some fuel rods;
- An active system of control rods that modulate reactivity (and power, temperatures, etc.) by insertion or extraction movements within the core. These rods are made of AgInCd alloy or steel, depending on the needed absorption efficiency.

Before conducting the design studies of the PRATIC core, it was essential to define several parameters to ensure alignment with those found in established industrial concepts and/or to integrate technological solutions already used in the nuclear industry. Among these parameters, the following are particularly noteworthy:

- The number of FA composing the core, which is based on the Chinese ACP100 concept (Danrong, Qing, Dong, Gaojian, & Chang, 2021);
- The core's total thermal power has been fixed to 350 MW_{th}. This power, slightly lower than the one of the ACP100 [(Yu, et al., 2020), (Xu, 2016)], allows to reduce the average linear power (115.97 W/cm), improving a safety margin relative to the fuel's melting point in particular when accidental transients will be considered;
- The pin configuration within the assemblies, following the standard design of UOX fuel assemblies used in the French fleet (Vuiart, Brovchenko, Taforeau, Jaiswal, & Dumonteil, 2022). The assemblies include a 17x17 pin layout, with 264 fuel rods, 24 guide tubes for control rod insertion, and a central guide tube for instrumentation (cf. Figure 1);

Co-funded by the European Union
UK Research and Innovation
The Research Council of Norway
Project funded by

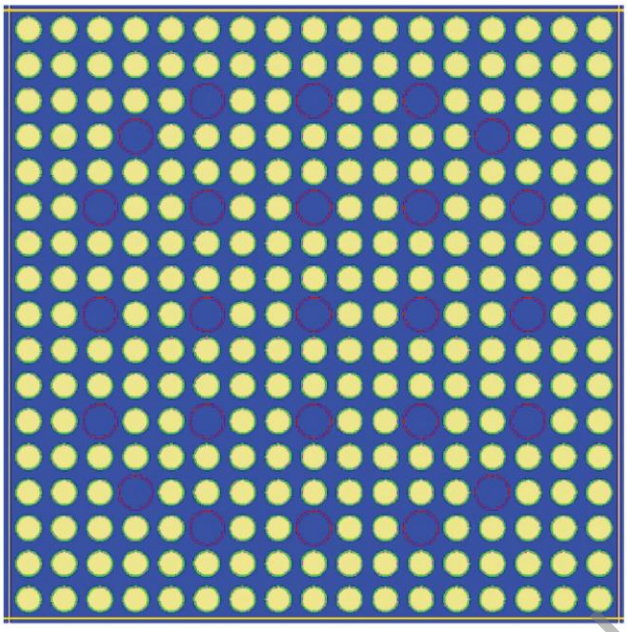

Figure 1: Radial cut of a 17x17 UOX fuel assembly. The UO2 fuel pellets are shown in yellow and their cladding in green. The instrumentation tube and guide tubes are represented by red circles filled with blue, which stands for water.

- The type of fuel, based on the classic solution for French enriched natural uranium (ENU) assemblies, i.e., UO_2 with uranium enriched in ^{235}U from natural content (0,7 % of ^{235}U) to 5%wt or less (CEA, 2008);
- The incorporation of gadolinium-poisoned fuel rods, aligning with a commonly employed solution in SBF-LW-SMRs designs (Yu, et al., 2020). All fuel rods containing gadolinium poison are made of a homogeneous mix of UO_2 and Gd_2O_3. Most of them feature a 8%wt gadolinium content and a 2.5%wt ^{235}U enriched UO_2 support, aligning with the composition of poisoned fuel rods outlined in (Pieck, 2013);
- The use of two types of absorber rod clusters: “grey” and “black” clusters. Grey clusters are made of 16 silver-indium-cadmium alloy (AgInCd = AIC) rods and 8 steel rods. Black clusters are made of 24 AIC rods;
- The cold active height (i.e., at 20°C) was arbitrarily set to 200 cm, so that the core is roughly as high as it is wide, thus minimizing neutron leakage;
- The moderator pressure in the primary circuit, set to 155 bars, corresponds to that of French PWRs (Grard, 2014). The moderator pressure is maintained constant across all core power levels;
- A neutron reflector mainly composed of steel, also referred to as "heavy reflector", is used in PRATIC. This type of reflector is selected for its ability to minimize neutron leakage at the core's edges, thereby extending the cycle length compared to a reflector mainly made of water. This technological solution is already utilized in some PWR-type SMRs, as noted in (Suk, Chvala, Maldonado, & Frybort, 2021);
- The moderator temperature program is designed to maintain an average core temperature of 300°C, with a temperature increase of 30°C across the active height of the core at full power (see Figure 21 page 36). This results in a moderator inlet temperature of 285°C (at nominal power) and a flow rate of 1 550 $kg \times m^{-2} \times s^{-1}$ (assuming there is no flow in the guide tube, see section 8.5.4 page 35). It also ensures the core remains isothermal at 300°C under hot zero power conditions. These parameters were chosen by the PRATIC designers without specific studies or sensitivity analysis but are similar to the thermal-hydraulic conditions found in PWR-type SMR concepts referenced in [(Small Modular Reactor Technology Catalogue, 2024), (The NEA Small Modular

Co-funded by the European Union
UK Research and Innovation
The Research Council of Norway
Project funded by

Reactor Dashboard: Second Edition, 2024)]. The moderator flow rate of 1 550 kg×m^{-2}×s^{-1} is maintained constant across all core power levels;
- The cycle ends when the core reactivity reserve reaches 100 pcm (for this benchmark, this end-of-cycle (EOC) criterion will not be retained, see section 8.6.2.2 page 40);
- The core operates on a 2-batch cycle, a strategy described in (Ingrumeau & Cordiez, 2015) as optimal for achieving a cycle length of approximately 2 years while maintaining a flat power distribution.

Then, a core was designed with the assumptions above, and using materials and geometries described in other PWR benchmarks, such as BEAVRS (Horelik, Herman, Forget, & Smith, 2013) in revision 3.0, or VERA (Godfrey, 2014) in revision 4. To do so, the PRATIC design team defined several core parameters, such as:
- Number of fuel assembly (FA) types and zoning of FAs within the core;
- Fuel enrichment in ^{235}U for each FA type;
- Number and characteristics of gadolinium-poisoned fuel pins for each FA type;
- Control scheme of the core (control rod arrangement within the core and management of the insertion / extraction);
- Definition of reflectors.

7.1.3. Main design criteria

To setup the above parameters, the guidelines followed by the design team were as follows:
- Try to reach the greater cycle length (near 2 years), while maintaining as low as possible the reactivity in "All Control Rods Out" (ARO) configuration during the irradiation cycle;
- Limit the 2D power peaking factor, named F_{XY}^{maxi}, to avoid the moderator boiling crisis;
- Limit the 3D power peaking factor, named F_{Q}^{maxi}, to avoid the fuel melting during some accident transients.

The formulas defining F_{XY} and F_Q for a mesh located at coordinates (x, y, z) are given below:

$$F_Q(x,y,z) = \frac{P_{th,vol}(x,y,z)}{P_{th,vol}^{AVE,core}}, \qquad F_Q^{maxi} = \max_{x,y,z} F_Q(x,y,z)$$

Equation 1: definition of F_Q and F_Q^{maxi}

Where:
- $P_{th,vol}(x,y,z)$ represents the thermal power density (W/cm^3) of the mesh located at coordinates (x,y,z), where x and y denote the coordinates in the (X,Y) plane, and z denotes the axial position along the z-axis;
- $P_{th,vol}^{AVE,core} = \sum_{X,Y,Z} \frac{V(x,y,z)\times P_{th,vol}(x,y,z)}{\sum_{X,Y,Z} V(x,y,z)}$ (expressed in W/cm^3). Here, $V(x,y,z)$ represents the volume (cm^3) of the mesh located at coordinates (x,y,z).

$$F_{XY}(x,y) = \frac{P_{th,surf}(x,y)}{P_{th,surf}^{AVE,core}}, \qquad F_{XY}^{maxi} = \max_{x,y} F_{XY}(x,y)$$

Equation 2: definition of F_{XY}

Where:
- $P_{th,surf}(x,y) = \sum_Z P_{th,vol}(x,y,z) \times \Delta z(x,y,z)$ (expressed in W/cm^2). Here, $\Delta z(x,y,z)$ denotes the height (cm) of the mesh located at coordinates (x,y,z);
- $P_{th,surf}^{AVE,core} = \sum_{X,Y} \frac{S(x,y)\times P_{th,surf}(x,y)}{\sum_{X,Y} S(x,y)}$ (expressed in W/cm^2). Here, $S(x,y)$ is the area (in cm^2) of the radial mesh located at coordinates (x,y).

Co-funded by the European Union
UK Research and Innovation
The Research Council of Norway
Project funded by

F_{XY}^{maxi} and F_Q^{maxi} are the maximal values of respectively F_{XY} and F_Q observed on the entire mesh. The F_Q is minimised in order to limit the maximal linear power, named P_{lin}^{maxi}, to a value of around 300 W/cm in normal operation, which is a value permitting to have a sufficiently safe behaviour during incident transients (class 2). The aim of this limit is to avoid fuel melting during this kind of transients, which can occur when the linear power reaches 590 W/cm. The experience feedback on other PWR designs shows that limiting the maximal linear power to 300 W/cm in normal operation conditions avoids reaching 590 W/cm in class 2 transients. The maximal linear power reached in a core is calculated with the equation below:

$$F_Q^{maxi} \times P_{lin}^{AVE,core} \leq P_{lin}^{maxi}$$

Equation 3: definition of the maximal linear power limit

The PRATIC core was designed with an average linear power at nominal conditions of $P_{lin}^{AVE,core} = 115.97\ W/cm$, so that, to respect a maximal linear power of $P_{lin}^{maxi} = 300\ W/cm$, the F_Q^{maxi} is limited to a value of approximately $F_Q^{maxi} = 2.587$.

The F_{XY} is limited to avoid reaching the water saturation in the hottest channel. An empiric safety margin of 15 % is taken in consideration to setup this limit. Thus, the calculation of the maximal value of F_{XY} is given by:

$$F_{XY}^{maxi} \leq F_{XY}^{\text{limit}} = (1 - 0.15) \times F_{XY}^{sat} \quad ,$$
$$F_{XY}^{sat} = \frac{\dot{m} \cdot Cp}{P_{th,core}} \times \left(T_{mod,sat} - T_{mod,in}\right) \quad ,$$

Equation 4: calculation formula of F_{XY} limit at saturation

Where:

- $\dot{m}$ is the water mass flow in the core (in kg×s^{-1});
- Cp represents the specific heat capacity of the moderator (in J×kg^{-1}×K^{-1});
- $P_{th,core}$ denotes the core thermal power (in W);
- $T_{mod,sat}$ is the liquid water temperature at vapor saturation (344.79°C at 155 bars);
- $T_{mod,in}$ is the core inlet temperature (in °C).

At nominal power (350 MWth), the core inlet temperature is set to $T_{mod,in} = 285°C$, so $F_{XY}^{sat} = 2.038$ and $F_{XY}^{limit} = 1.732$. This value of F_{XY}^{limit} fixes a limit to the maximal moderator temperature value to 335.8°C, which is 9°C under the saturation temperature.

7.1.4. Designed cores

Two cores were designed with the above assumptions and criteria.

The first to be designed was the **equilibrium cycle core**. To obtain it, a calculation of the fuel depletion during an irradiation cycle is carried out, until the reserve of reactivity reaches 100 pcm[(1)] (i.e., k_{eff} = 1.001 with all absorbing rods fully extracted). Then, half of the fuel assemblies is discharged and replaced by fresh fuel assemblies, and the other half is reloaded into the core. A new depletion calculation is performed, ending with the same reloading. A calculation loop called "rise to equilibrium" has been set up until the depletion calculation converges to the same behaviour. As soon as the difference in cycle length from one calculation to the previous one does not exceed a small value, the loop is broken and the search for

(1) This EOC criterion has been chosen during the design phase of PRATIC core, but it is not relevant for this benchmark (see section 8.6.2.2 page 40)

Co-funded by the European Union
UK Research and Innovation
The Research Council of Norway
Project funded by

equilibrium ends. At this stage, the designers chose the value of 15 MWd/ton[2] as a stopping criterion for the equilibrium. The last cycle of this calculation loop is considered as the equilibrium cycle.

After that, the objective was to design a **start-up core**, composed of only fresh fuel assemblies. Indeed, benchmark activities are easier when the composition of the fuel is well known by all the benchmark partners, without any ambiguity. This is not the case for the equilibrium cycle core, because at the beginning of the cycle, half of the fuel assemblies has been irradiated during one cycle. As a result, all participants need to perform depletion calculations, which may lead to variations in fuel composition at BoC when reloading assemblies, potentially making it difficult to explain discrepancies between results. Thus, it is better to begin a benchmark with a core composed of only fresh fuel assemblies. This situation is encountered during the first cycle, also called the start-up core. The fuel assembly loading map for this core must be different than those of the equilibrium core because fresh fuel assemblies have a higher reactivity than depleted fuel assemblies. To account for this, 2nd-cyle fuel assemblies must be replaced by fresh fuel assemblies containing a lower amount of fissile material. The new fresh fuel assemblies were designed to primarily satisfy the safety criteria (2D and 3D power peaking factors), and try to obtain a cycle length not so far from the equilibrium cycle length. This led to the definition of the start-up core V1 which consists of 7 different types of fuels assemblies: 3 types of assemblies identical to those used in the equilibrium core, and 4 additional types are set specific to the start-up core.

In order to simplify the definition of the start-up core, a new release called **start-up core V2** was designed, containing only 5 fuel assembly types. However, at full power, this core had no margin regarding the safety criteria at the beginning of cycle. Thus, the decision was to begin the irradiation cycle with a gradual power increase: starting at 7.5 % Nominal Power (NP) at the beginning of cycle (BOC), to reach 100 % NP at 2 GWd/t. This progressive power level ramp-up allows the safety criteria on F_{XY}^{maxi} and F_{Q}^{maxi} to be satisfied with sufficient margins.

7.2. Revision notes

The data of the PRATIC benchmark is detailed in two Excel Workbooks, which are available in a GIT repository. Access to this repository can be requested via email at: pratic@cea.fr.

- PRATIC_EquilibriumCycleCore_InputDataFile_VX.Y.xlsx for the equilibrium cycle core;
- PRATIC_StartUpCore_InputDataFile_VX.Y.xlsx for the start-up core.

X.Y denotes the revision number of the file. This document has been written based on the revision number 1.8 of the “equilibrium file” and the revision number 2.0 of the “start-up file”.

[2] This criterion is not relevant for this benchmark, as it risks to introduce unwanted discrepancies in the partners’ results. It has been transformed into a number of irradiation cycles to simulate (see section 8.6.2.3 page 40).

Co-funded by the European Union
UK Research and Innovation
The Research Council of Norway
Project funded by

8.Specifications of the PRATIC benchmark

This section defines the specification of the PRATIC benchmark, *i.e.*, the input data needed to calculate the benchmark. For both cores, start-up and equilibrium, the specifications are provided at full power (*i.e.*, 100 % NP) assuming that there is no geometry nor material modification between 0 % NP and 100 % NP, except the water density. This lead to consider all the **dimensions and densities at 300 °C for all operating conditions**. For information only, materials and geometries considered at 20°C are given in appendix (cf. Section 11).

8.1. Nuclear data library

In order to avoid unnecessary discrepancies between the results of the partners, it is better to define a common nuclear data library. During the kick-off meeting of the EASI-SMR project (24 – 25 September 2024, Palaiseau, France), it appeared that most of the partners could perform calculations with the ENDF/B-VII.1 nuclear data library (Chadwick, et al., 2011).
Although PRATIC was initially designed with the JEFF-3.1.1 library, the EASI-SMR benchmark will be realized with **ENDF/B-VII.1**.

8.2. Material compositions and isotopic densities

This section provides the isotopic definition of the materials used in the benchmark. Some explanations and details are given in the appendix (see section 11), but the material data to be used for the benchmark is the content of section 8.2. As explained at the beginning of section 8, all materials except water have the same definition for each operating condition. Fuel materials are the only materials that deplete (i.e., in particular, we do not consider depletion of AIC and SS-304 absorber rods). The materials given in this section are only fresh materials (i.e., the isotopic concentrations of depleted fuels must be calculated by each partner of the benchmark).

8.2.1. Fuel materials

Several fuel types are used in the PRATIC cores:

- Standard fuels are uranium oxide UO_2;
- Poisoned fuels are gadolinium oxide mixed with uranium oxide UO_2-Gd_2O_3.

All fuels are low-enriched uranium (LEU: $^{235}U \leq 5$ %wt.) made with UNE. The primary difference between fuels lies in the initial enrichment $\boldsymbol{w}$ of the ^{235}U isotope. The quantity of ^{234}U and ^{236}U in the fuel are deducted from this $\boldsymbol{w}$ value, using the formulas found in (Godfrey, 2014) p. 18 and reproduced in table 1.

Table 1: LEU isotopic equations

Isotope	Equation
U-234	$0.007731 \times \boldsymbol{w}^{1.0837}$
U-235	$\boldsymbol{w}$
U-236	$0.0046 \times \boldsymbol{w}$
U-238	Balance

The numeric application of the equations given in table 1 to the fuels found in the PRATIC cores give the values reported in table 2. In tables 2 to 4, the columns in blue correspond to fuels present in both start-up and equilibrium cores, while columns in yellow represent fuels that are only loaded in the start-up core.

Table 2: LEU isotopic weight percent (%wt.)

Enrichment in U235 / Isotope	1.6%	2.5%	2.8%	3.5%	5.0%
U234	0.013	0.021	0.024	0.030	0.044
U235	1.600	2.500	2.800	3.500	5.000
U236	0.007	0.011	0.013	0.016	0.023
U238	98.380	97.468	97.163	96.454	94.933

For all 5 standard fuels described in table 2, the fuel density is assumed to be the same. By using the effective density of ideal cylindrical fuel pellets at 20°C (cf. Section 11.1.1 page 47) and the thermal expansion law of UO_2 (cf. Section 11.3 page 50), we determine the **effective density of UO_2 at 300°C to 10.1711 g/cm^3** (this value is also reported in table 35 page 52). This value is assumed to be constant for all fuel temperatures[3] (the fuel temperature coefficient is assumed to change only the neutron cross sections resonances by Doppler broadening effect, not the material density).

Knowing the effective density of UO_2, the isotopic densities at the beginning of life (BOL) are calculated and their values are reported in table 3.

Table 3: Isotopic densities of standard fuels at 300°C and BOL (Expressed in atom/barn/cm)

Enrichment in U235 / Isotope	1.6%	2.5%	2.8%	3.5%	5.0%
O16	4.5373E-02	4.5377E-02	4.5379E-02	4.5383E-02	4.5390E-02
U234	2.9682E-06	4.8143E-06	5.4434E-06	6.9324E-06	1.0203E-05
U235	3.6755E-04	5.7429E-04	6.4320E-04	8.0399E-04	1.1485E-03
U236	1.6836E-06	2.6305E-06	2.9462E-06	3.6827E-06	5.2608E-06
U238	2.2314E-02	2.2107E-02	2.2038E-02	2.1877E-02	2.1531E-02

Most of the gadolinium-poisoned fuels used in both start-up and equilibrium cores contain 8 %wt. of Gd_2O_3 and 92 %wt. of UO_2. However, there is an exception for some gadolinium-poisoned fuel pins loaded in the start-up core, which are composed of 2 %wt. of Gd_2O_3 and

[3] For example, if we consider a fuel mesh located near the bottom of the active zone, at full power. In this example, the fuel temperature is supposed to be 350 °C, and the other components (cladding, water) are at 285 °C. The **geometries of all the elements** (fuel and cladding radius, cell and assembly pitch) are those considered at **300 °C**. The **density of water** in this mesh is adapted to its particular situation: in this example, **285°C** and 155 bars. The **density of the other elements** (fuel, cladding, etc.) remains the same as described at **300 °C**. The **neutron cross sections** of each material are adapted to the particular situation: the cross sections of **fuel** are defined at **350 °C**, those of **cladding and water** are defined at **285 °C**.

Co-funded by the European Union
UK Research and Innovation
The Research Council of Norway
Project funded by

98 %wt. of UO_2. For both types of gadolinium-poisoned fuel, the densities at 20°C are calculated in table 28 page 48. Then, the thermal expansion coefficients reported in table 34 page 52 are applied, and give the values of the density of the mix between UO_2 and Gd_2O_3 for several temperatures in table 35 page 52 in the Appendices section. **At 300°C**, these densities are worth **9.8003 g/cm^3 for 8% gadolinium** in poisoned fuel and **10.0797 g/cm^3 for 2% gadolinium** in poisoned fuel. In all cases, the ^{235}U initial enrichment of LEU that compose UO_2-Gd_2O_3 is 2.5 %wt. Finally, the isotopic densities of the gadolinium-poisoned fuels at the beginning of life (BOL) are given in table 4. These values will change during irradiation.

Table 4: Isotopic densities of gadolinium-poisoned fuels at 300°C and BOL (in atom/barn/cm)

Gd_2O_3 mass ratio / Isotope	2.0%	8.0%
Gd152	1.3396E-06	5.2100E-06
Gd154	1.4602E-05	5.6790E-05
Gd155	9.9134E-05	3.8554E-04
Gd156	1.3711E-04	5.3325E-04
Gd157	1.0483E-04	4.0769E-04
Gd158	1.6638E-04	6.4709E-04
Gd160	1.4642E-04	5.6946E-04
O16	4.5075E-02	4.4133E-02
U234	4.6756E-06	4.2677E-06
U235	5.5774E-04	5.0908E-04
U236	2.5547E-06	2.3319E-06
U238	2.1470E-02	1.9597E-02

8.2.2. Fuel cladding materials

The fuel cladding is made of Zircaloy-4. Knowing its elemental composition (cf. Table 29 p. 48) and assuming a density of **6.5215 g/cm^3 at 300 °C** (cf. Table 35 p. 52), the isotopic densities are calculated and presented in table 5. This material is also used in guide tubes and instrument tube of fuel assemblies.

Co-funded by the European Union
UK Research and Innovation
The Research Council of Norway
Project funded by

Table 5: Isotopic densities of Zircaloy-4 at 300°C

Isotope	Atom density (atom/barn/cm)
Cr50	3.2818E-06
Cr52	6.3287E-05
Cr53	7.1762E-06
Cr54	1.7863E-06
Fe54	8.6321E-06
Fe56	1.3551E-04
Fe57	3.1294E-06
Fe58	4.1647E-07
O16	3.0692E-04
Sn112	4.6532E-06
Sn114	3.1661E-06
Sn115	1.6310E-06
Sn116	6.9750E-05
Sn117	3.6842E-05
Sn118	1.1619E-04
Sn119	4.1207E-05
Sn120	1.5629E-04
Sn122	2.2210E-05
Sn124	2.7775E-05
Zr90	2.1733E-02
Zr91	4.7393E-03
Zr92	7.2442E-03
Zr94	7.3413E-03
Zr96	1.1827E-03

8.2.3. Structural material

The designers of PRATIC chose AISI 304 austenitic stainless steel (also named SS-304) as a structural material. This grade of stainless steel is used in reflectors, serves as cladding for neutron absorber rods, and is also used as low-effect neutron absorber in grey control rods. Knowing the elemental composition (cf. Table 30 p. 49) and assuming a density of **7.9181 g/cm^3 at 300 °C** (cf. Table 35 p. 52), the isotopic densities are calculated and presented in table 6.

Co-funded by the European Union
UK Research and Innovation
The Research Council of Norway
Project funded by

Table 6: Isotopic densities of AISI 304 at 300°C

Isotope	Atom density (atom/barn/cm)
Cr50	7.5708E-04
Cr52	1.4600E-02
Cr53	1.6555E-03
Cr54	4.1208E-04
Fe54	3.4137E-03
Fe56	5.3588E-02
Fe57	1.2376E-03
Fe58	1.6470E-04
Mn55	1.7359E-03
Ni58	5.5307E-03
Ni60	2.1304E-03
Ni61	9.2608E-05
Ni62	2.9528E-04
Ni64	7.5198E-05
Si28	9.3954E-04
Si29	4.7705E-05
Si30	3.1447E-05

8.2.4. Neutron absorber materials

In PRATIC core, neutron absorbers are made of two main materials: AIC and SS-304.

AIC, also named AgInCd is a silver-indium-cadmium alloy often used in control rods. In PRATIC core, this material is used in black and in grey control rods. The weight fractions of elements are given in table 31 p. 49 and **the density at 300 °C is assumed to be 9.9849 g/cm^3** (cf. Table 35 p. 52). Consequently, the isotopic densities at 300 °C are calculated in table 7.

Table 7: Isotopic densities of AIC at 300°C

Isotope	Atom density (atom/barn/cm)
Ag107	2.3118E-02
Ag109	2.1478E-02
Cd106	3.3432E-05
Cd108	2.3804E-05
Cd110	3.3405E-04
Cd111	3.4234E-04
Cd112	6.4537E-04
Cd113	3.2683E-04
Cd114	7.6840E-04
Cd116	2.0033E-04
In113	3.3685E-04
In115	7.5187E-03

SS-304, also named AISI 304, is already described in section 8.2.3 Structural material. This material is present in grey control rods, where some AIC rods are replaced by SS-304 to reduce the neutron absorbing effect compared to AIC. SS-304 is also used as cladding for neutron absorber rods (same cladding material for both AIC and SS-304 rods). Moreover, SS-304 is present in upper, lower, and radial reflector regions.

Co-funded by the European Union
UK Research and Innovation
The Research Council of Norway
Project funded by

For the PRATIC benchmark the neutron absorber materials, both **AIC and SS-304**, are assumed to be static materials. It means that we **do not consider depletion** for these materials.

8.2.5. Other materials

This section describes water and helium materials.

Water is used as a moderator in PRATIC reactor core, to slow down neutrons thus maintaining the fission chain reaction. It is also used as a coolant, permitting heat transfer from the core to steam generator. PRATIC is a soluble boron free design, so boric acid is not present in this core. For reasons of model simplicity, the PRATIC benchmark does not consider any spacer grid in the core. For all these reasons, PRACTIC water is assumed to be composed only by hydrogen and oxygen isotopes, in stoichiometric proportions: two atoms of hydrogen $^{1}_{1}H$ for one atom of oxygen $^{16}_{8}O$.
To correctly account for neutron scattering, it is advised to use cross sections including thermal scattering law $S(\alpha, \beta)$ of hydrogen linked to oxygen. For that reason, in this document, hydrogen-linked-to-oxygen is noted H1_H2O.
The density of liquid water is linked to temperature, pressure, and enthalpy in water tables. The PRATIC core was designed with CRONOS2 code (Lautard, Loubière, & Feudon-Magnaud, 1992), which is based on the same water tables as FLICA4 thermal-hydraulics code (Toumi, Bergeron, Gallo, Royer, & Caruge, 2000). Both CRONOS2 and FLICA4 are deterministic codes developed at CEA. Table 8 supplies some examples of isotopic densities of H1_H2O and O16 for several pairs of pressure and temperature values. In this table, the density of water is calculated using CRONOS2 – FLICA4 water tables, but each code can have its own water tables. This could imply some slight discrepancies between the definitions of water material made by different codes.

Table 8: Isotopic densities of water for several pressure and temperature conditions, as calculated by the CRONOS2-FLICA4 codes

Pressure (bar)	**155**	**155**	**155**	**155**	**1**
Temperature (°C)	285	300	315	20	20
Density (g/cm³)	7.5572E-01	7.2683E-01	6.9325E-01	1.0051E+00	9.9823E-01
Isotope	Isotopic density (atom/barn/cm)				
H1_H2O	5.0538E-02	4.8606E-02	4.6360E-02	6.7217E-02	6.6755E-02
O16	2.5269E-02	2.4303E-02	2.3180E-02	3.3608E-02	3.3377E-02

The second material described in this section is helium. This material is present in the gap between the fuel pellet and the cladding, and in the gap between the neutron absorber rod and its cladding. helium gas is assumed to be at a pressure of 2 MPa and a temperature of 600 K, resulting in an assumed density of ρ_{He} =0.0015981 g/cm³ at 300 °C [(Horelik, Herman, Forget, & Smith, 2013), pp. 48 and 141 of the revision 3.0 of this document, dated from July, 14th 2020]. The isotopic densities are given in table 9.

Table 9: Isotopic densities of helium gas at 300°C and 2 MPa

Isotope	**Atom density (atom/barn/cm)**
He3	4.8089E-10
He4	2.4044E-04

Co-funded by the European Union
UK Research and Innovation
The Research Council of Norway
Project funded by

8.3. Geometries

This section provides the geometric definition of the elements used in the benchmark. Some explanations and details are given in the appendix (see section 11), but the geometric data to be used for the benchmark is the content of section 8.3. As explained at the beginning of section 8, the geometric definition of the elements (cell, assembly, core) is unchanged for each operating condition.

The following sections are a hierarchical description of the core, like Russian dolls: the core is made up of fuel assemblies, themselves made up of cells. The sections below are organized from the most elementary parts to the overall description of the core.

8.3.1. Cell geometries

All fuel assemblies are made up of 6 types of cells:

- Standard fuel cell ("standard fuel cell", see figure 2 and table 10);
- Gadolinium-poisoned fuel cell ("gadolinium cell", see figure 2 and table 10);
- Empty guide tube cell ("guide tube cell", see figure 3 and table 11);
- AgInCd inserted into guide tube cell ("AIC cell", see figure 4 and table 13);
- Stainless steel inserted into guide tube cell ("SS-304 cell", see figure 4 and table 13);
- Empty instrument tube cell ("instrument cell", see figure 3 and table 12).

The geometries of the standard and gadolinium-poisoned fuel cells are identical. The geometries of the AIC and SS-304 fuel cells are almost identical. The only difference between these two pairs of cells is the material of the inner part of the cell (and a slight difference in the inner rod radius, negligible in the case of fuels). The geometries of the empty guide tube and instrumented tube cells are also similar, although they do not have the same dimensions. Figures 2 to 4 give a schematic representation of these three pairs of cells.

Figure 2: Standard and gadolinium-poisoned fuel cells representation

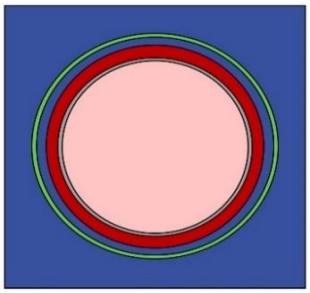

Figure 4: AIC and SS-304 cells representation

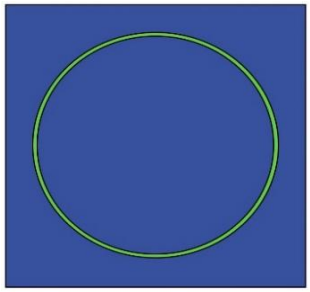

Figure 3: Empty guide tube and instrument tube representation

Co-funded by the European Union
UK Research and Innovation
The Research Council of Norway
Project funded by

The dimensions at 300 °C of these cells are provided in tables 10 to 13.
For information, dimensions at 20 °C are given in appendix (see section 11.2). Values at 300 °C are obtained by applying the thermal expansion laws described in section 11.3 to the values at 20 °C shown in table 32, considering a free-constraint dilation hypothesis (*i.e.*, without considering the out/in pressure gradient, no cladding creep, etc.). The cell pitch values at 300 °C were determined by using the Zy4 dilatation coefficient.

Table 10: Standard and gadolinium-poisoned fuel cells dimensions at 300 °C

Element	Value at 300 °C	Unit	Filling material
Fuel pellet radius	0.4107	cm	UO_2 or $UO_2Gd_2O_3$
Inner clad radius	0.4186	cm	He
Outer clad radius	0.4757	cm	Zy4
Cell pitch	1.2618	cm	H_2O

Table 11: Empty guide tube cell dimensions at 300 °C

Element	Value at 300 °C	Unit	Filling material
Inner guide tube radius	0.5618	cm	H_2O
Outer guide tube radius	0.6029	cm	Zy4
Cell pitch	1.2618	cm	H_2O

Table 12: Empty instrument tube cell dimensions at 300 °C

Element	Value at 300 °C	Unit	Filling material
Inner instrument tube radius	0.5598	cm	H_2O
Outer instrument tube radius	0.6059	cm	Zy4
Cell pitch	1.2618	cm	H_2O

Table 13: Absorber inserted into guide tube cell dimensions at 300 °C

Element	Value at 300 °C	Unit	Filling material
Absorber rod radius	0.3844	cm	AgInCd or SS-304
Inner cladding radius	0.3879	cm	He
Outer cladding radius	0.4863	cm	SS-304
Inner guide tube radius	0.5618	cm	H_2O
Outer guide tube radius	0.6029	cm	Zy4
Cell pitch	1.2618	cm	H_2O

8.3.2. Assembly geometries

Fuel assemblies are composed of **17×17 cells**, surrounded by a **water gap**. A schematic 2D representation of a fuel assembly slice is provided in figure 1 page 10.
An **instrument tube** is at the central position of the assembly: for this benchmark, the instrument tubes will always remain empty (*i.e.*, filled with water) because the instrumentation of the core is not modelled.
Figure 1 shows 24 other cells that look like the instrument tube: these are **guides tubes**, whose role is to ensure a certain mechanical rigidity to the assembly and to allow the insertion of core reactivity control clusters.
These **control rod clusters** are made of 24 absorber pins that can move axially in the guide tubes. The insertion of a control rod cluster into the core reduces reactivity (*i.e.*, attenuates the fission chain reaction), and the extraction rise the reactivity (*i.e.*, amplifies the fission chain reaction).

Two types of control rod clusters are defined in the PRATIC core: **grey** and **black** clusters. Grey control rod clusters (see figure 17) are made of 8 SS-304 pins and 16 AIC pins whereas black clusters are made of 24 AIC pins. As the SS-304 absorption efficiency is lower than that of the AIC, the grey control rod clusters are less efficient than the black ones. This definition of control clusters is intended to allow fine or coarse control of reactivity.

The section 8.3.4.2 page 26 shows that the core is composed of 3 zones, whose assembly layouts are depicted from figure 6 to figure 10:

- **Central**; this zone contains only one fuel assembly (identical for the start-up core and the equilibrium core) that includes 8 gadolinium poisoned pins (see figure 6);
- **Internal**, this zone contains one assembly type loaded in both start-up and equilibrium core (see figure 7), and another assembly type that is only loaded in the start-up core (see figure 8);
- **External**, this zone contains one assembly type loaded in both start-up and equilibrium core (see figure 9), and another assembly type that is only loaded in the start-up core (see figure 10).

Co-funded by the European Union
UK Research and Innovation
The Research Council of Norway
Project funded by

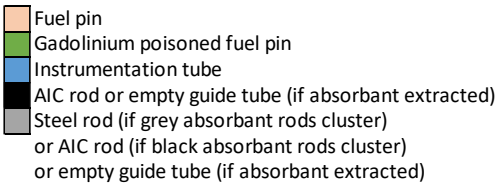

Figure 5: Caption for figures 6 to 10

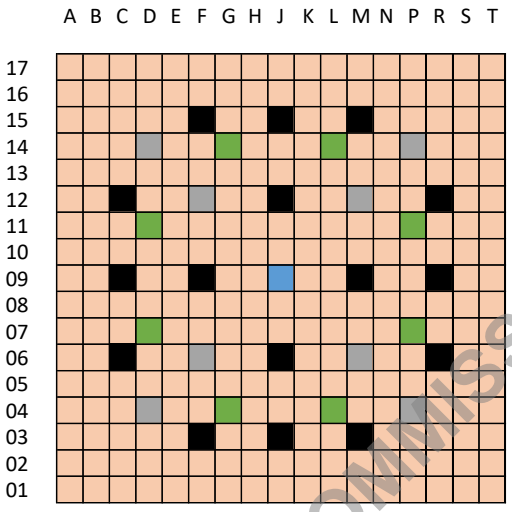

Figure 6: "central" assembly layout with 8 gadolinium fuel pins

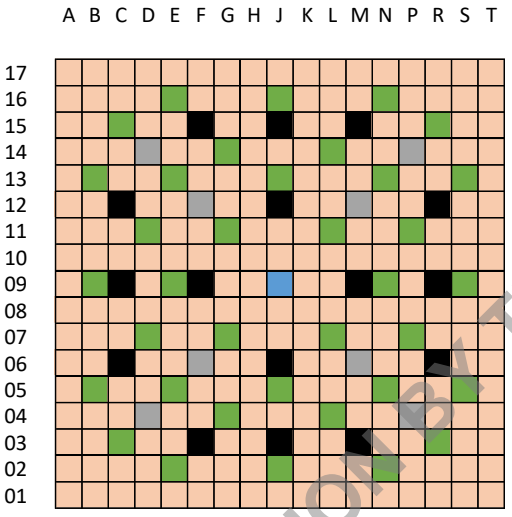

Figure 7: "internal" assembly layout with 36 gadolinium fuel pins – corresponds to "internal 1" locations in the start-up core

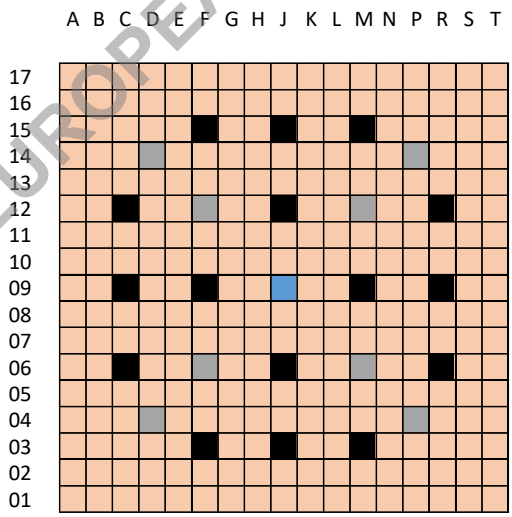

Figure 8: "internal 2" assembly layout without gadolinium fuel pin (only loaded in start-up core)

Co-funded by the European Union
UK Research and Innovation
The Research Council of Norway
Project funded by

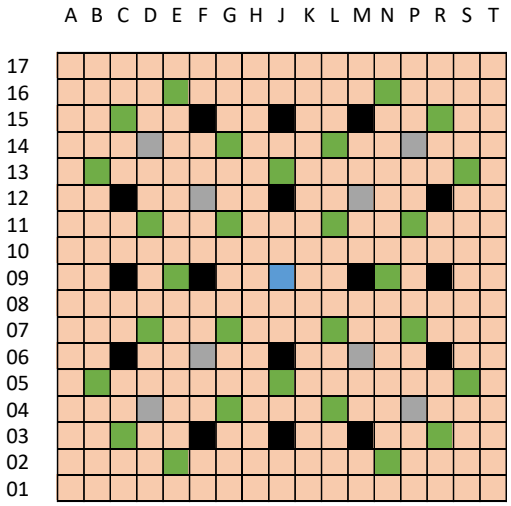

Figure 9: "external" assembly layout with 28 gadolinium fuel pins – corresponds to "external 1" locations in the start-up core

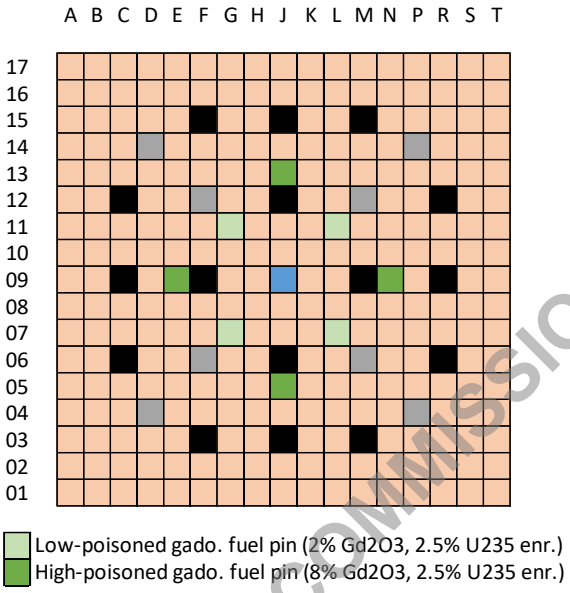

Figure 10: "external 2" assembly layout with 8 gadolinium fuel pins (only loaded in start-up core)

The geometric features of the fuel assemblies are provided in table 14 at 300 °C. As explained before, these values are assumed to be constant for all operating conditions. It can be noted that the inter-assembly half-gap of 0.04035 cm, present on each side of the assembly, is included in the assembly pitch value (21.5313 cm). These values at 300°C were determined from the values at 20°C described in table 32 page 50, and the thermal expansion coefficients detailed in section 11.3. As for the cell pitch, the assembly pitch and subsequent inter-assembly half-gap at 300°C are determined using the dimensions at 20°C and the coefficient of thermal expansion of the Zy4.

Table 14: Fuel assembly dimensions at 300 °C

Element	Value at 300 °C	Unit
Cell pitch	1.2618	cm
Assembly pitch	21.5313	cm
Inter-assembly half gap	0.04035	cm
Active height	200.5613	cm

8.3.3. Reflectors

8.3.3.1. Radial reflector

In order to minimize neutron leakages – thus extending at maximum the cycle length – and to flatten the radial power distribution in the active zone, designers of PRATIC chose a radial reflector mainly made of steel. This type of reflector is the one used by EPR design, for example. As explained in (AREVA Design Control Document, revision 5, September 2013), the heavy reflector reduces the fast flux on the pressure vessel and improves the neutron economy in the active core. Water has a strong negative effect on fast neutron reflector and must be minimized in heavy steel reflectors. However, it is necessary to cool-down the heavy reflector by adding cooling channel into. With a volume ratio of approximately 95% metal to 5% water, the heavy reflector efficiently reflects fast neutrons back to the fuel.

Co-funded by the European Union
UK Research and Innovation
The Research Council of Norway
Project funded by

The PRATIC designers chose to model the radial reflector as a homogeneous material, made up of **95 %vol. of SS-304 and 5 %vol. of water**. The active zone of the core is surrounded by a row of 'reflector blocks', each block being the size of a fuel assembly, as shown in figure 11. Outside these blocks, a **void boundary condition** is applied.

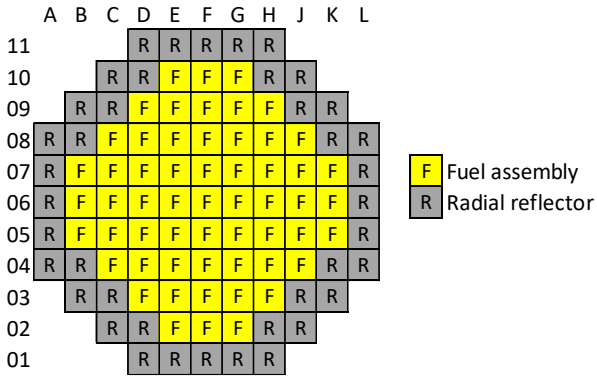

Figure 11: Radial cut of the PRATIC core

N.B.: to simplify the model, there is no water gap in the radial reflector zone and the positions of the water holes used for reflector cooling are not defined (*i.e.*, homogeneous model).

8.3.3.2. Upper and lower axial reflectors

To simplify the model, upper and lower axial reflectors are assumed to be identical. PRATIC designers made the following procedure to define the axial reflectors:

- Imagine a 2D-plane representation of a fuel assembly;
- Absorber rods are inserted inside guide tubes;
- The areas of fuel pins (clad outer radius) + absorber rods (clad outer radius) + guide tube (Zy4 ring) + instrument tube (Zy4 ring) are assumed to be made of **steel** (SS-304): the sum of these areas represents **45.14 %vol.** of the fuel assembly total area (see table 15);
- The remainder of the fuel assembly geometry (**54.86 %vol.**) is made up of **water**.

The detailed definition of homogeneous axial reflectors is given in table 15. We can remark that absorber materials are replaced by steel. This means that PRATIC designers assumed to not model the neutron absorbers in the upper axial reflector (see section 8.3.4.4).

Co-funded by the European Union
UK Research and Innovation
The Research Council of Norway
Project funded by

Table 15: Definition of homogeneous axial reflectors

Object	Value at 300°C	Unit
Assembly pitch	21.5313	cm
Total surface of an assembly	463.5969	cm^2
Number of fuel pin per assembly	264	
Outer fuel cladding radius	0.4757	cm
Surface of fuel pin per assembly	187.6743	cm^2
Number of guide tube per assembly	24	
Outer absorber cladding radius	0.4863	cm
Inner guide tube radius	0.5618	cm
Outer guide tube radius	0.6029	cm
Surface of guide tube + absorber	21.4400	cm^2
Number of instrument tube	1	
Inner instrument tube radius	0.5598	cm
Outer instrument tube radius	0.6059	cm
Surface of instrument tube	0.1688	cm^2
Total surface of water per assembly	254.3138	cm^2
Volume fraction of water in axial reflectors	54.86%	
Volume fraction of steel (SS-304) in axial reflectors	45.14%	

The thickness of both axial reflectors is assumed to be 20 cm, with a void boundary condition at the top and bottom ends of the reflectors.

8.3.4. Core geometries

8.3.4.1. Axial mesh

The axial definition of PRATIC is very simple (see figure 12), and especially because there is no heterogeneity in the active zone. This means the same fuel material is used throughout the active height, and that spacer grids are not modelled. From the top to the bottom, we find at 300 °C:

- 20 cm of upper axial reflector;
- 200.5613 cm of active zone;
- 20 cm of lower axial reflector.

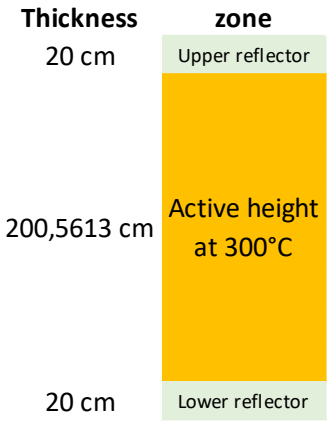

Figure 12: Schematic view of the axial geometry of PRATIC

8.3.4.2. Core zoning

The PRATIC core is composed of 57 fuel assemblies (FAs), distributed in 3 zones that remain identical for both the start-up and equilibrium cores:

Co-funded by the European Union
UK Research and Innovation
The Research Council of Norway
Project funded by

- **Central**, this zone only concerns the FA located at the center of the core;
- **Internal**, this zone concerns 16 FAs surrounding the central one;
- **External**, this zone concerns 40 FAs at the periphery of the core.

A view of this core zoning is shown in figure 13. The role of this zoning is to flatten the neutron flux and power distributions within the core.

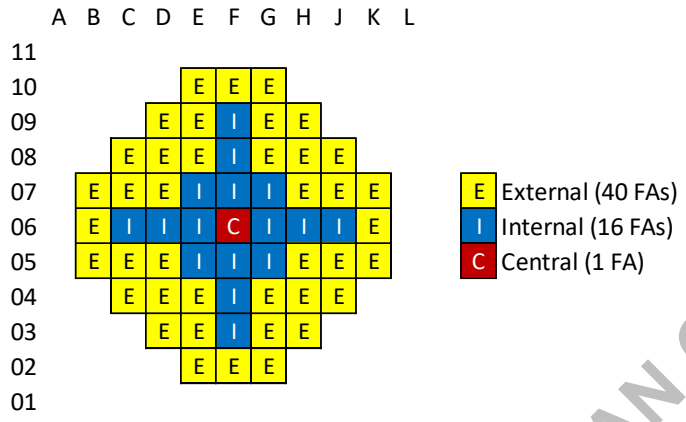

Figure 13: Core zoning of start-up and equilibrium cores

8.3.4.3. Fuel assemblies loading patterns

In order to flatten the neutron flux and power distribution, the loading pattern of the fuel assemblies within the core zoning alternates between assemblies with a high and a low level of reactivity. Firstly, this is achieved by defining fuel assemblies with high and low fissile material content. In addition, the variation of the gadolinium content within the fuel assemblies is used to adjust their reactivity level at their BOL. After one irradiation cycle, all the gadolinium is consumed, and the reactivity value increases most of the time.

In the start-up core, this alternation of high and low reactivity level assemblies is achieved by defining two types of fuel assemblies in each zone: one with a high ^{235}U enrichment and a large amount of gadolinium, and the other with low enrichment and low quantity of gadolinium. In the equilibrium core (used from the second irradiation cycle onwards), this alternation of high and low reactivity level assemblies is due to the use of first and second cycle fuel assemblies.

As a reminder, the term 'start-up core' is used to define the first irradiation cycle, which is initially loaded with fresh fuel only. The term 'equilibrium core' is used to define all subsequent irradiation cycles where the loading at the beginning of the cycle is half fresh assemblies (29 assemblies) and half assemblies irradiated during the previous cycle (28 assemblies).

Co-funded by the European Union
UK Research and Innovation
The Research Council of Norway
Project funded by

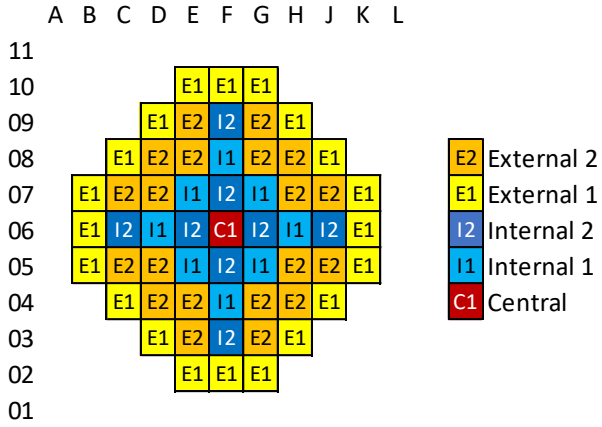

External 2 Fuel Assemblies = UOX 2,8% ; 4 Gd pins w/ 2% Gd_2O_3 + 4 Gd pins w/ 8% Gd_2O_3
External 1 Fuel Assemblies = UOX 5,0% ; 28 Gd pins w/ 8% Gd_2O_3
Internal 2 Fuel Assemblies = UOX 1,6% ; 0 Gd pin
Internal 1 Fuel Assemblies = UOX 3,5% ; 36 Gd pins w/ 8% Gd_2O_3
Central Fuel Assembly = UOX 2,5% ; 8 Gd pins w/ 8% Gd_2O_3

Figure 14: Assembly loading pattern of the start-up core

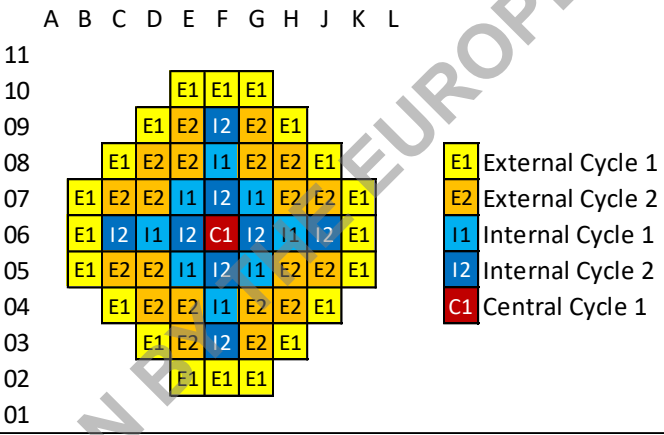

External Fuel Assemblies = UOX 5,0% 28Gd
Internal Fuel Assemblies = UOX 3,5% 36Gd
Central Fuel Assembly = UOX 2,5% 8Gd

Figure 15: Assembly loading pattern of the equilibrium core

The movements of fuel assemblies operated during the transition from one cycle to another are defined in section 8.6.3 Fuel management, page 40.

8.3.4.4. Rod Control cluster assemblies

The control of the core reactivity is realised by the rod control cluster assemblies (RCCA). RCCA are made of 24 absorber rods, cladded with SS-304 material, which can be inserted into the guide tubes of fuel assemblies. The level of insertion or extraction of absorber rods in the fuel assembly determines the level of neutron absorption, and therefore makes it possible to control the reactivity and power of the core. In the PRATIC core, the RCCA only control reactivity and power; there is no control of axial offset nor temperature distribution shape.

This insertion level can vary:

Co-funded by the European Union
UK Research and Innovation
The Research Council of Norway
Project funded by

- from 0 cm of insertion; in that case the lower base of the absorber rods is aligned with the top fuel level (see figure 16 on the left);
- to 200 cm of insertion; in that case, the lower base of the absorber rods is almost aligned with the bottom fuel level (actually due to axial thermal expansion of the active zone, the lower base of absorbers are 0.5613 cm above the bottom fuel level, see figure 16 on the right).

The designers of PRATIC assumed that RCCAs are not modelled in the upper reflector, so inserting a 0 cm RCCA into the core is the same as not representing that RCCA. They also assume that the reference level of RCCAs (corresponding to a 0 cm of insertion) is always the plan between the top of the active zone, and the bottom of the upper axial reflector. To simplify the model, the insertion or extraction movements of control rods do not take into account any thermal expansion (1 cm of insertion is no more than 1 cm of insertion). That is why there is a 0.5613 cm thickness at the bottom of the active zone where the control and shutdown rods will never be inserted.

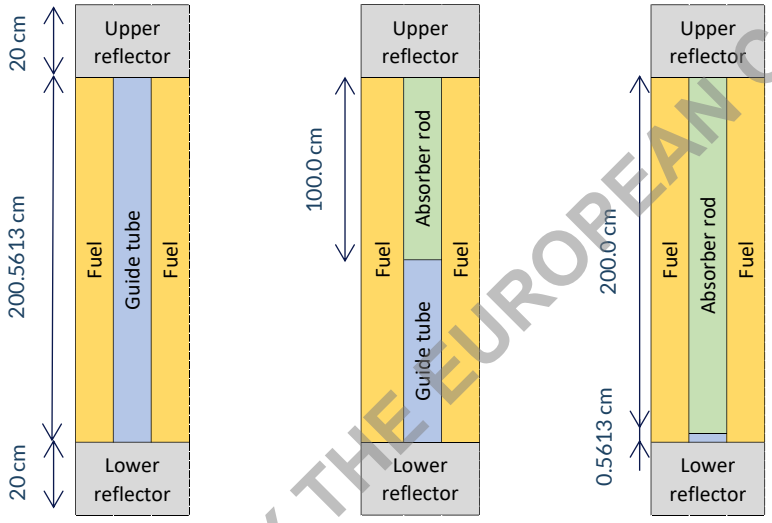

Figure 16: Absorber rod insertion axial scheme (left: 0 cm of insertion "rod fully extracted"; center: 100 cm of insertion "mid-insertion of rod"; right: 200 cm of insertion "rod fully inserted")

The definition of the RCCA system is the same for both start-up and equilibrium cores. Two types of RCCAs are used for fine or coarse control of core reactivity (see figure 17):

- **Black** RCCAs are made up of **24 AIC** rods for broad reactivity control;
- **Grey** RCCAs consist of **16 AIC** rods and **8 SS-304** rods for fine reactivity control.

Co-funded by the European Union
UK Research and Innovation
The Research Council of Norway
Project funded by

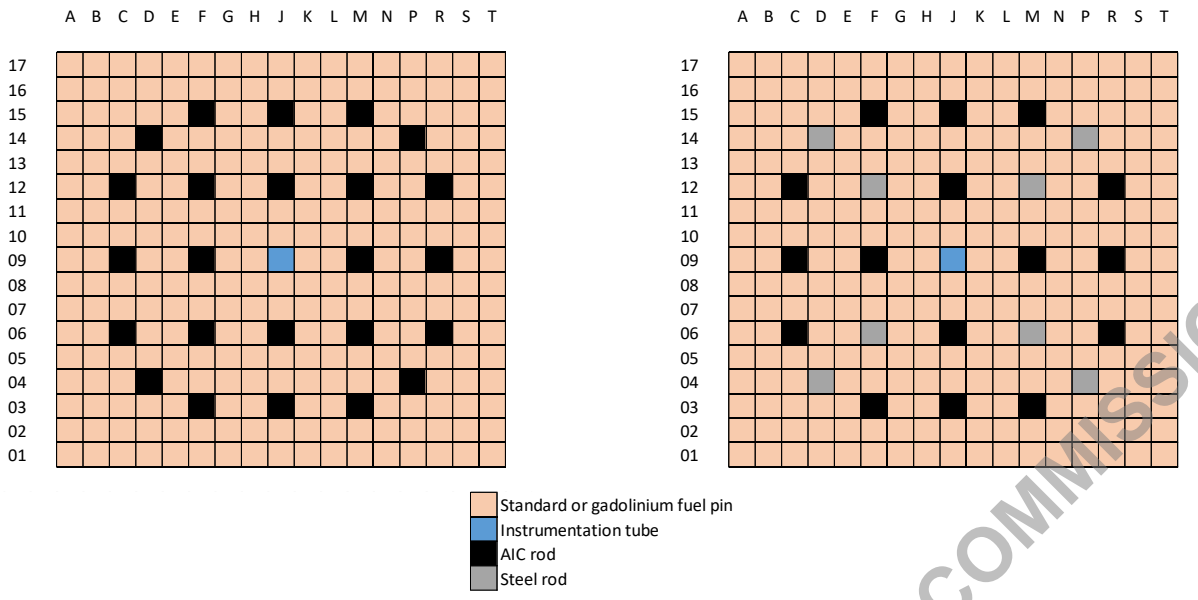

Figure 17: Assembly layout of the RCCAs in the fuel assembly (black RCCA is on the left and grey RCCA is on the right)

PRATIC is a soluble boron-free reactor, so reactivity control requires the installation of an RCCA above each fuel assembly (RCCAs cover 100 % of fuel assemblies). The RCCAs are grouped into several banks with different functions: the first two are used to control the reactor, while the third is used for shutdown (see Figure 18).

- 3 grey control rod banks (G1, G2, G3), each consisting of 4 or 8 grey RCCAs;
- 1 black control rod bank (G4), comprising 4 black RCCAs;
- 1 shutdown rod bank involving 33 black RCCAs.

Each bank consists of RCCAs located at symmetrical positions within the core, so as to maintain quarter-core symmetry by rotation for the neutron flux. All RCCAs of one bank move together, so the insertion level of a single bank's RCCAs is always the same.

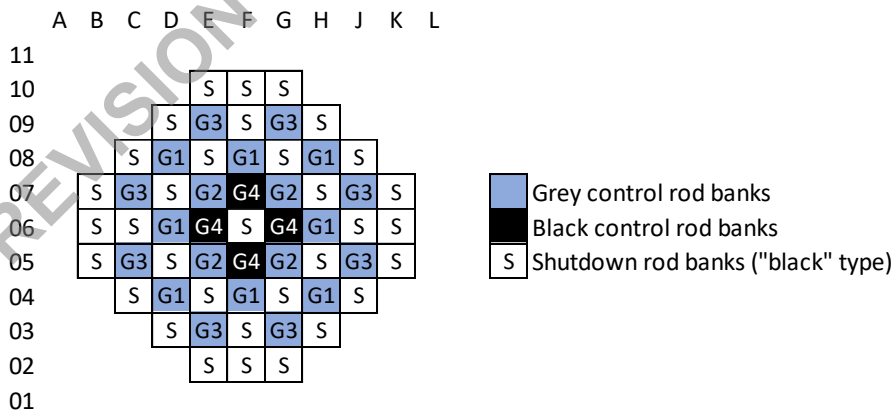

Figure 18: Location of RCCA banks within the core

It is worth mentioning that 42% of PRATIC assemblies incorporate rod clusters used for core control, and that 35% of the rod clusters loaded in the core (including shutdown rods) are grey rod clusters.

Co-funded by the European Union
UK Research and Innovation
The Research Council of Norway
Project funded by

8.4. Core and fuel assembly features

After the definitions of materials and geometries of PRATIC core, some fuel assembly and core features are given in this section.

8.4.1. Fuel assembly features

The general fuel assembly features are summarized in table 16.

Table 16: General fuel assembly features

Fuel assembly features	Value	Unit	Remark
Number of fuel assembly in the core	57	/	/
Size of the fuel pin cartesian lattice	17×17	/	/
Number of guide tubes per assembly	24	/	/
Number of instrument tube per assembly	1	/	/
Number of fuel pin per assembly	264	/	/
Assembly pitch at hot state	21.5313	cm	Value at 300°C
Inter-assembly half gap at hot state	0.04035	cm	Value at 300°C
Active height at hot state	200.5613	cm	Value at 300°C
Representation of spacer grids	no	/	/

By combining the data provided in the "Materials" (Section 8.2) and in the "Geometries" (see section 8.3) sections, the fuel assembly features can be calculated, for the start-up core (see table 17), and for the equilibrium core (see table 18).

Table 17: Technical characteristics of start-up core fuel assemblies

Type of assembly	1	2	3	4	5
Position of assembly in the core	central	internal 1	internal 2	external 1	external 3
Name of assembly	U250_8Gd	U350_36Gd	U160_0Gd	U500_28Gd	U280_8Gd
number of assembly in the core	1	8	8	20	20
U235 enrichment (weight%)	2.50%	3.50%	1.60%	5.00%	2.80%
number of gadolinium pins - type 1	8	36		28	4
number of gadolinium pins - type 2					4
number of UO_2 pins	256	228	264	236	256
Gd_2O_3 content in type 1 pin (weight%)	8%	8%		8%	2%
Gd_2O_3 content in type 2 pin (weight%)					8%
Density of UO_2 at 300°C (g/cm3)	10.1711	10.1711	10.1711	10.1711	10.1711
Average Mass Number of U in UO_2	237.9745	237.9440	238.0020	237.8982	237.9654
U content in UO_2 (weight%)	88%	88%	88%	88%	88%
Volume of UO_2 at 300°C (cm3)	27207	193852	224461	501636	544147

Co-funded by the European Union
UK Research and Innovation
The Research Council of Norway
Project funded by

Type of assembly	1	2	3	4	5
Density of UO_2-Gd_2O_3 type 1 at 300°C (g/cm^3)	9.8003	9.8003		9.8003	10.0797
Density of UO_2-Gd_2O_3 type 2 at 300°C (g/cm^3)					9.8003
Average Mass Number of U in UO_2-Gd_2O_3 type 1	237.9745	237.9745	237.9745	237.9745	237.9745
Average Mass Number of U in UO_2-Gd_2O_3 type 2					237.9745
U content in UO_2-Gd_2O_3 type 1 (weight%)	81%	81%	88%	81%	86%
U content in UO_2-Gd_2O_3 type 2 (weight%)	0%	0%	0%	0%	81%
Volume of UO_2-Gd_2O_3 type 1 at 300°C (cm^3)	850	30608		59516	8502
Volume of UO_2-Gd_2O_3 type 2 at 300°C (cm^3)					8502
Weight of U (g)	250687	1981237	2012449	4970297	5020180

Table 18: Technical characteristics of equilibrium core fuel assemblies

Type of assembly	1	2	3
Position of assembly in the core	central	internal	external
Name of assembly	U250_8Gd	U350_36Gd	U500_28Gd
number of assembly in the core	1	16	40
U235 enrichment (weight%)	2.50%	3.50%	5.00%
number of gadolinium pins	8	36	28
number of UO_2 pins	256	228	236
Gd_2O_3 content in fuel (weight%)	8%	8%	8%
Density of UO_2 at 300°C (g/cm^3)	10.1711	10.1711	10.1711
Average Mass Number of U in UO_2	237.9745	237.9440	237.8982
U content in UO_2 (weight%)	88%	88%	88%
Volume of UO_2 at 300°C (cm^3)	27207	387705	1003272
Density of UO_2-Gd_2O_3 at 300°C (g/cm^3)	9.8003	9.8003	9.8003
Average Mass Number of U in UO_2-Gd_2O_3	237.9745	237.9745	237.9745
U content in UO_2-Gd_2O_3 (weight%)	81%	81%	81%
Volume of UO_2-Gd_2O_3 at 300°C (cm^3)	850	61217	119032
Weight of U (g)	250687	3962473	9940594

The core produces 350 MW of thermal power. This value allows to determine some useful data for depletion calculations, provided in table 19. The total initial mass of uranium in the core is the sum of the last rows of tables 17 and 18.

Table 19: Data useful for fuel depletion calculations

Core concerned	Data	Value	Unit	Remark
Both start-up and equilibrium	Nominal thermal power [NP]	3.50E+08	W	/
Start-up core	Total initial mass of U in the core	1.42E+07	g	/
	Specific mass power	24.59	W/g	Used to normalize neutron flux in depletion calculations
Equilibrium core	Total initial mass of U in the core	1.42E+07	g	/
	Specific mass power	24.73	W/g	Used to normalize neutron flux in depletion calculations

8.4.1. Core features

Some general core features are provided in the table 20.

Table 20: General features of the core

	Value	Unit	Remark
Nominal thermal power [NP]	3.50E+08	W	/
Average linear power at 100%NP	115.97	W/cm	/
Specific mass power	24.59	W/g	Start-up core
Specific mass power	24.73	W/g	Equilibrium core
Average power density of fuel at 100%NP	218.85	W/cm^3	Volume considered is only those of fuel pellets
Average power density of core at 100%NP	66.04	W/cm^3	Volume considered is the whole volume of the active zone (fuel+clad+water)

8.5. Thermal model and thermal-hydraulics assumptions

The assumptions described in this section only concern the normal operating conditions. Some values may be reconsidered for incidental transient analysis.

8.5.1. Thermal conductivities

8.5.1.1. Thermal conductivity of fuels

The thermal conductivity law used for uranium-oxide fuels (both standard and gadolinium-poisoned) at normal operating conditions up to 1 900 K is the Lucata's law (Lucata, Matzke, & Hastings, 1996), derived from Harding and Martin's law (Harding & Martin, 1989) corrected from the effect of the fuel porosity.

Co-funded by the European Union
UK Research and Innovation
The Research Council of Norway
Project funded by

Lucata's law is expressed by equation 5, where λ is the thermal conductivity of the fuel expressed in W/m/K, λ_0 (see equation 6) is the Harding's expression for the thermal conductivity of unirradiated UO_2, and κ_{XX} are correction coefficients to account for irradiation. For thermal conductivity of PRATIC fuels, only the κ_{2p} correction term, giving the effect of porosity and fission-gas bubbles in fuel is accounted for:

$$\lambda = \kappa_{1d}\kappa_{1p}\kappa_{2p}\kappa_{3x}\kappa_{4r}\lambda_0 \,.$$

Equation 5: Lucata's law of thermal conductivity for uranium oxide fuels

In equation 6, T represents the temperature of the fuel in Kelvin. This equation is valid for a range of temperatures between 773 and 3 120 K, but we assume it valid from 273 to 3 120 K.

$$\lambda_0 = \frac{1}{0.0375 + 2.165 \times 10^{-4} \times T} + \frac{4.715 \times 10^9}{T^2} \times \exp\left(-\frac{16361}{T}\right)$$

Equation 6: Harding's expression of thermal conductivity of unirradiated UO_2

In equation 7, the porosity is chosen to p =5 % and the form factor is chosen to σ =1.5, which permits to represent a half-lived fuel.

$$\kappa_{2p} = \frac{1-p}{1+(\sigma-1)p}$$

Equation 7: Correction term giving the effect of porosity and fission-gas bubbles

A graphic view of Lucata's law expressed in equation 5 is given in the figure 19.

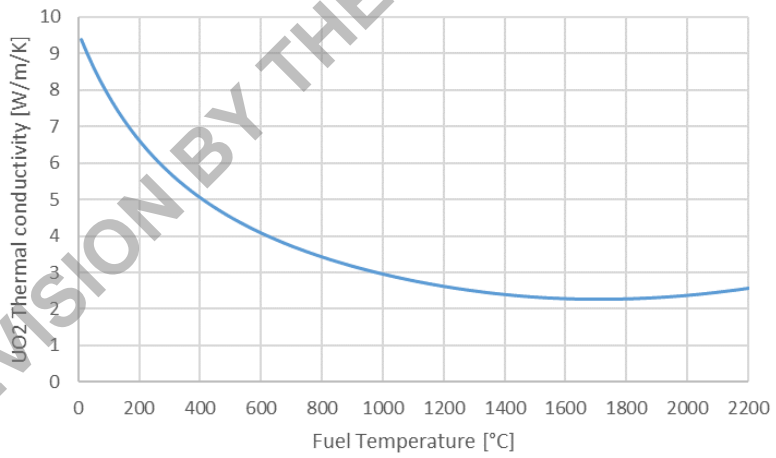

Figure 19: Lucata's law, thermal conductivity of UO_2

8.5.1.2. *Thermal conductivity of cladding*

The thermal conductivity of the Zircaloy-4 (Zy4) cladding is taken from the MATPRO handbook (Hagrman & Reymann, 1979), page 217, and expressed in equation 8 with λ the thermal conductivity expressed in W/m/K and T the temperature of the clad in kelvin:

$$\lambda = 7.51 + 2.09 \times 10^{-2} \times T - 1.45 \times 10^{-5} \times T^2 + 7.67 \times 10^{-9} \times T^3$$

Equation 8: Thermal conductivity law of the Zircaloy-4 cladding

Figure 20 shows the variation of the Zy4 thermal conductivity as a function of the cladding temperature.

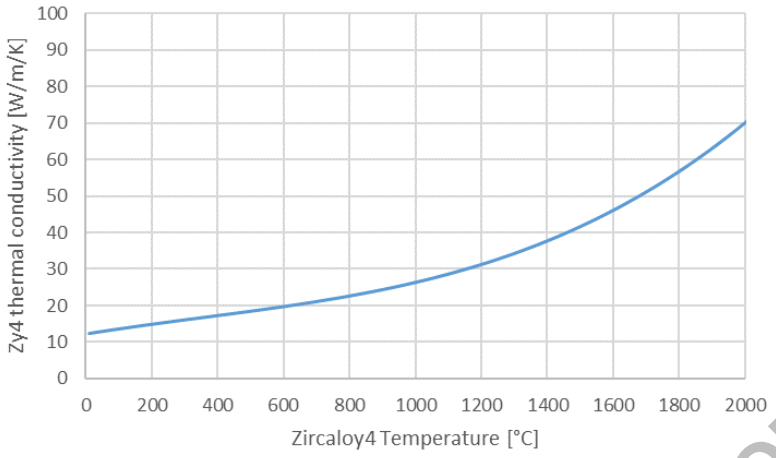

Figure 20: Zircaloy4 thermal conductivity

8.5.2. Pellet-clad gap conductance

The gap between the fuel pellets and their clad is filled with helium. The thermal model used to represent this gap is assumed to be independent on the gap thickness. Therefore, this gap is described by a conductance value named H_{gap}. To simplify the thermal model definition, this value is assumed constant for every burnup value, every linear power of the fuel, and every core operating condition. PRATIC designers chose the value below, corresponding to an averaged H_{gap} value along a fuel cycle.

$$H_{gap} = 1\ \mathrm{W/(cm^2 \times °C)}$$

Equation 9: Constant value considered for the conductance of the gap between fuel pellet and its clad

This value of H_{gap} is the same for both start-up and equilibrium cycles, and is the same for standard and gadolinium-poisoned fuel pins.

8.5.3. Energy deposition

The assumptions described in this section are applicable for both start-up and equilibrium cores.

To simplify the thermal-hydraulic model, the energy produced by **neutron capture in non-fissile areas is not taken into account**. This only concerns the reflectors, the instrument, and guide tubes (with or without control rod inserted).

In other areas (*i.e.*, fuel areas), power is produced by fission and capture reactions. It is assumed that 96.5 % of the total power is deposited in the fuel pellets, 1 % in their cladding and 2.5 % of this power is deposited directly in the moderator.

8.5.4. General thermal-hydraulic features

The general thermal-hydraulic features of the PRATIC core are detailed in table 21. They are applicable for both start-up and equilibrium cores. The moderator flow rate is chosen to produce a temperature difference ΔT between the bottom and the top of the fissile height of 30 °C at nominal power (NP = 350 MWth). This moderator flow rate is converted into several units in

table 21. To simplify the model, it is assumed that there is no moderator flow inside the guide tubes (the moderator inside the guide tubes is assumed not to move), and no bypass has been defined, so the moderator flow rate described in the table below concerns only the moderator circulating around the fuel pins.

Table 21: General thermal-hydraulic characteristics of the PRATIC core

	Value	Unit	Remark
Nominal thermal power [NP]	3.50E+08	W	/
Moderator pressure in the primary circuit	155	bars	
Moderator cross section in the core at 300°C	1.41	m^2	Assuming that the moderator circulates around the fuel rods only (not in the guide tubes)
Density of water at 155 bars and 300°C	726.83	kg/m^3	Value considered in CRONOS2 / FLICA4 codes from CEA
Moderator flow rate in the core (same value expressed in 3 different units)	1550.00 2185.39 10824.28	$kg/m^2/s$ kg/s m^3/h	Effective core flow (not including bypass, assuming no flow in guide tubes), assumed to be constant for each power level Calculated at 155 bars and 300°C, assumed to be constant for each power level
Conductance of the fuel-clad gap	1.00	$W/(cm^2 \times °C)$	This value is assumed to be a constant (in space, in burnup and in power level)

The moderator flow rate is assumed to be constant under all operating conditions. Therefore, variations in power imply variations in the inlet and outlet moderator temperatures as shown in figure 21. This diagram also shows that the moderator mean temperature (calculated as the mean value between the inlet and outlet temperatures) is constant under all operating conditions.

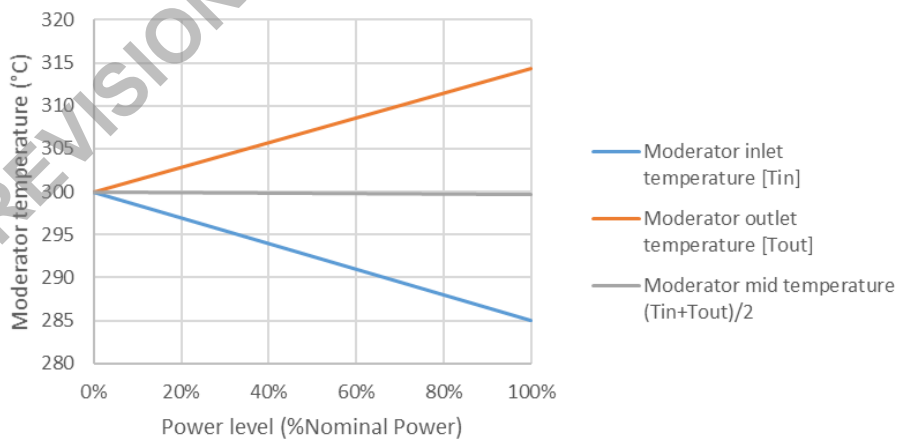

Figure 21: Operating temperatures diagram

Examples of temperatures, calculated by CEA with the CRONOS2 code (and its simplified thermal-hydraulic model called THERMOC) are given in tables 22 and 23, respectively at hot full power and hot zero power conditions, at the BOC of the equilibrium core.

Table 22: Operating conditions at hot full power (100 %NP)

Operating conditions at 100%NP	Value	Unit	Remark
Moderator pressure	155,00	bars	/
Moderator inlet temperature [T_{in}]	285,00	°C	/
Moderator outlet temperature [T_{out}]	314,32	°C	average of meshes in the upper active plane, at the beginning of equilibrium cycle
Moderator 3D averaged temperature	302,30	°C	averaged 3D moderator density, converted into temperature, at beginning of equilibrium cycle
Moderator mean temperature (T_{in}+T_{out})/2	299,66	°C	/
Fuel 3D averaged temperature	470,55	°C	CRONOS2 calculations, at the beginning of equilibrium cycle

Table 23: Operating conditions at hot zero power (0 %NP)

Operating conditions at 0%NP	Value	Unit	Remark
Moderator pressure	155,00	bars	/
Moderator inlet temperature [T_{in}]	300,00	°C	/
Moderator outlet temperature [T_{out}]	300,00	°C	/
Moderator 3D averaged temperature	300,00	°C	/
Moderator mean temperature (T_{in}+T_{out})/2	300,00	°C	/
Fuel 3D averaged temperature	300,00	°C	/

8.6. Reactor management and control

This section describes how the banks of control rods are inserted into the core in relation to each other, what defines the end of a cycle and how the fuel assemblies are reloaded in the next cycle, as well as the management of core power during irradiation cycles.

8.6.1. Absorber banks diagram

Section 8.3.4.4 gives a definition of RCCAs that are used to control the reactivity of the core. They are grouped into banks to perform different functions: control of the reactivity and power, and shutdown of the core. Within a bank, all control clusters are inserted at the same level into the core. The clusters are symmetrically distributed in the core to maintain a symmetrical distribution of neutron flux and power.

The simultaneous insertion of all banks at the same level will push the neutron flux towards the lower part of the core, resulting in an increase in the power factors in this zone, and in particular the F_Q^{maxi} factor (see section 7.1.3 Main design criteria, page 11). With a regular distribution of

cluster groups within the core, the F_{XY}^{maxi} factor is then generally fairly low. On the contrary, waiting for one group of clusters to be fully inserted before inserting another will reduce 3D power factor F_{Q}^{maxi} but will increase 2D power factor F_{XY}^{maxi}.

For PRATIC, a compromise was found by defining a cluster group overlap rate of 50% for banks G2 to G4. This means that bank n° X starts to be inserted into the core when bank n° X-1 is inserted by 50% of its length. In practice, as the insertion length of the clusters is 200 cm, a RCCA bank starts to move when the previous bank exceeds the value of 100 cm of insertion in the core. Since the cluster insertion speeds are identical for all the banks, the two banks then insert the same length simultaneously. The absorber insertion diagram of banks G1 to G4 is shown in figure 22. This diagram and all this section are relevant for both start-up and equilibrium cores.

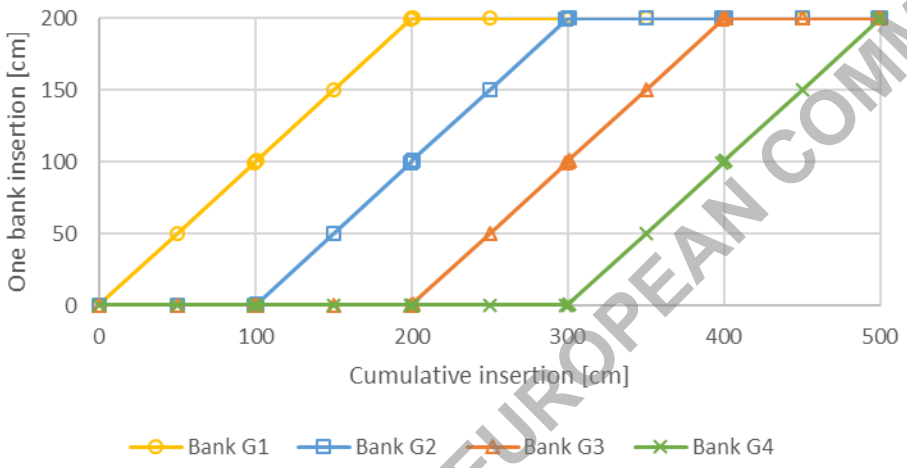

Figure 22: Absorber banks insertion diagram

The respect of this overlap of 50 % between RCCA banks means that the insertion level of all the banks can be known with a single value, called the "cumulative insertion level". Knowing all the RCCA bank insertion levels (marked I_{G1} to I_{G4}), this cumulative insertion level (marked I_{cumul}) is calculated using equation 10:

$$I_{cumul} = \min(I_{G1}\,;\,50\% \times 200) + \min(I_{G2}\,;50\% \times 200) + \min(I_{G3}\,;50\% \times 200) + I_{G4}$$

Equation 10: Definition of the cumulative insertion level

The reciprocal formulae for determining the insertion levels of groups G1 to G4 as a function of the cumulative insertion level are detailed in the system of equation 11.

$$\begin{cases} I_{G1} = \min(I_{cumul}\,;200) \\ I_{G2} = \min(max(0\,;I_{cumul} - 50\% \times 200)\;;200) \\ I_{G3} = \min(max(0\,;I_{cumul} - 100\% \times 200)\;;200) \\ I_{G4} = \min(max(0\,;I_{cumul} - 150\% \times 200)\;;200) \end{cases}$$

Equation 11: Correspondence between individuals and cumulative insertion levels

Using equations 10 or 11, the values in table 24 can be used as examples.

Co-funded by the European Union
UK Research and Innovation
The Research Council of Norway
Project funded by

Table 24: Examples of RCCA banks insertion

Insertion [cm]				
Cumulative insertion	Bank G1	Bank G2	Bank G3	Bank G4
0	0	0	0	0
50	50	0	0	0
99	99	0	0	0
100	100	0	0	0
101	101	1	0	0
150	150	50	0	0
199	199	99	0	0
200	200	100	0	0
201	200	101	1	0
250	200	150	50	0
299	200	199	99	0
300	200	200	100	0
301	200	200	101	1
350	200	200	150	50
399	200	200	199	99
400	200	200	200	100
401	200	200	200	101
450	200	200	200	150
499	200	200	200	199
500	200	200	200	200

The minimal insertion or extraction step of RCCAs is worth 1 cm, so we can consider that individual and cumulative insertion level values expressed in centimetres are integer values.

8.6.2. Definition of the irradiation cycle and achieving equilibrium

8.6.2.1. Xenon saturation

During an irradiation cycle, depletion calculations of the fuels (standard and gadolinium-poisoned) are performed. Many isotopes are created by fission or by the decay of fission products. Among them, $^{135}_{54}Xe$ matters on the neutron balance because its neutron capture cross section is very large. Its depletion chain is given in (Cacuci, 2010), p. 1252, and recalled in figure 23. ^{135}Xe is a fission product and also appears after a ^{135}I β-decay; it disappears by neutron capture or β-decay. As shown in figure 23, arrivals or removals of ^{135}Xe by β-decay have a decay period of some hours. In order to simplify the model, the saturation concentration of ^{135}Xe will be calculated for each fuel mesh of the core calculation, and at each time step of the depletion calculation. The saturation (also called "equilibrium") concentration of ^{135}Xe is determined with the help of the local neutron flux level inside each mesh.

$$\underset{\uparrow \text{Fission}}{Te^{135}} \xrightarrow[<0.5\,\text{min}]{\beta} I^{135} \xrightarrow[6.7hr]{\beta} \underset{\uparrow \text{Fission}}{Xe^{135}} \xrightarrow[9.2hr]{\beta} Cs^{135} \xrightarrow[2.6x10^6 yr]{\beta} Ba^{135}\,(stable)$$

Figure 23: Depletion chain of Xe135

Co-funded by the European Union
UK Research and Innovation
The Research Council of Norway
Project funded by

8.6.2.2. End of cycle criterion

During the design phase of PRATIC, depletion calculation were performed until the reactivity capacity of the core reached of fell below 100 pcm. The reactivity capacity is the difference between the ARO (All Rods Out) and CRI (Critical Rods Insertion) configurations.

This criterion is not relevant for a benchmark, as each partner will have a different depletion calculation, with a large dispersion in cycle length results. In order to limit this dispersion, it was decided to fix the cycle length limits at given values, based on estimates from CEA and IRSN pre-calculations using the JEFF-3.1.1 and ENDF/B-VII.1 nuclear data libraries. Thus, the cycle length determined for the **start-up core** is **16 GWd/t** and that for **subsequent cycles** (2nd cycle, 3rd cycle, etc.) is set at **17.5 GWd/t**.

In theory, the neutron simulations of all the partners should be over-critical (i.e. the core should be able to be maintained criticality by inserting the control rods) up to these burnup values. If this is not the case, the core will be maintained in ARO configuration, and the depletion calculation will continue until the target burnup is reached.

8.6.2.3. Achieving equilibrium cycle

After each irradiation cycle, one-half of the fuel assemblies is discharged and replaced by fresh fuels, and the other half is reloaded (see section 8.6.3). Cycle after cycle, the depleted fuel reaches an asymptotic isotopic distribution at EOC. This generally results in cycle lengths that converge cycle after cycle towards the same value. During the design phase of PRATIC, a difference of 15 MWd/t from one cycle to the next triggered the achievement of this equilibrium.

As the cycle lengths are fixed, this criterion is not relevant for this benchmark. The objective of this benchmark is to provide a common simulation framework for all partners, in order to compare results during incident transient scenarios simulated with neutronics and thermal-hydraulics coupled code systems. It does not matter whether the equilibrium is achieved or not. This benchmark is therefore limited to the simulation of 4 irradiation cycles:

- the **1st cycle** with the **start-up core** up to a burnup of **16 GWd/t**;
- the **following 3 cycles** with the **equilibrium core** up to a burnup of **17.5 GWd/t**.

8.6.3. Fuel management

After each irradiation cycle of the equilibrium core, one-half of the fuel assemblies (29 FAs) is discharged and replaced by fresh fuels, and the other half (28 FAs) is reloaded. The very first cycle is special in that it contains only fresh fuels, and hence specific assemblies dedicated to the start-up core. Nevertheless, the locations of discharged FAs after the irradiation cycle of start-up or equilibrium cycles remain the same and are presented in figure 24. It can be noted that the location of discharged FAs of the start-up core correspond to the specific FAs dedicated to this core. Consequently, from the second cycle onwards, the definition of the core corresponds to that of the equilibrium core.

Co-funded by the European Union
UK Research and Innovation
The Research Council of Norway
Project funded by

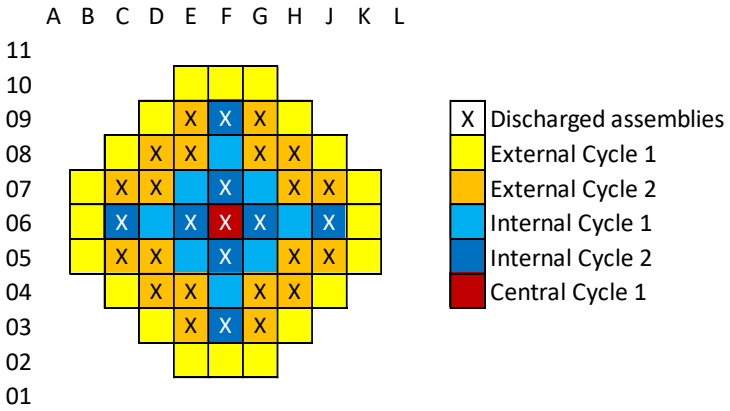

Figure 24: Location of discharged fuel assemblies

During the fuel reloading, the FAs that have been irradiated during one cycle are moved to a new location within the core corresponding to a "cycle-2 location". Fresh FAs will take place within the core in "cycle-1 locations". This core refuelling pattern is shown in figure 25 and is relevant for every inter-cycle (i.e., between cycles 1 and 2, 2 and 3, 3 and 4, etc.). An empty FA location means that this FA is a fresh one. A filled coordinate within a FA location indicates the location of this FA during the previous cycle. The refuelling pattern is designed to ensure quarter-core symmetry (by rotation) of the fuel assemblies.

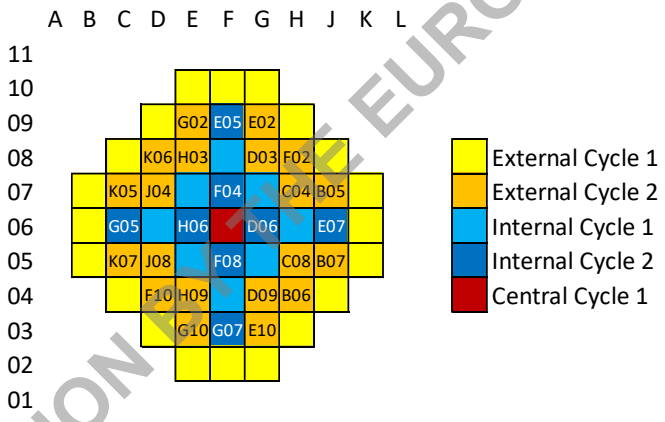

Figure 25: Core refuelling pattern

8.6.4. First core power increase

The equilibrium core is considered at nominal power (100 %NP = 350 MWth) from the beginning to the end of cycle.

This assumption is an issue for the start-up core, because it is loaded with only fresh fuels. Despite the definition of specific FAs with low-enriched uranium within the start-up core, the first power peaking factors calculated at 100 %NP shown a non-respect of the safety criteria (in particular F_{XY}^{maxi}) at the BOC (until 2 GWd/t). For this reason, it was decided to reduce the power at the very beginning of the first cycle and to gradually increase the power until 100 %NP is reached at a core burn-up of 2 GWd/t. This power ramp-up of the start-up core is described in table 25 and figure 26. During this step-up, some parameters of the core remain constant:

- The moderator pressure is worth 155 bars;
- The moderator flow rate is worth 1 550 kg/m^2/s;
- The moderator average temperature, calculated by the mean between inlet and outlet temperature is worth 300 °C.

Co-funded by the European Union
UK Research and Innovation
The Research Council of Norway
Project funded by

Table 25: Start-up core power step-up values

Step	Burnup start [MWd/t]	Burnup end [MWd/t]	Relative power level (%Nominal power)	Moderator inlet temperature (°C)	Moderator outlet temperature (°C)
1	0	150	7,5	298,875	301,125
2	150	500	25	296,25	303,75
3	500	1000	50	292,5	307,5
4	1000	2000	75	288,75	311,25
5	2000	End of Cycle	100	285	315

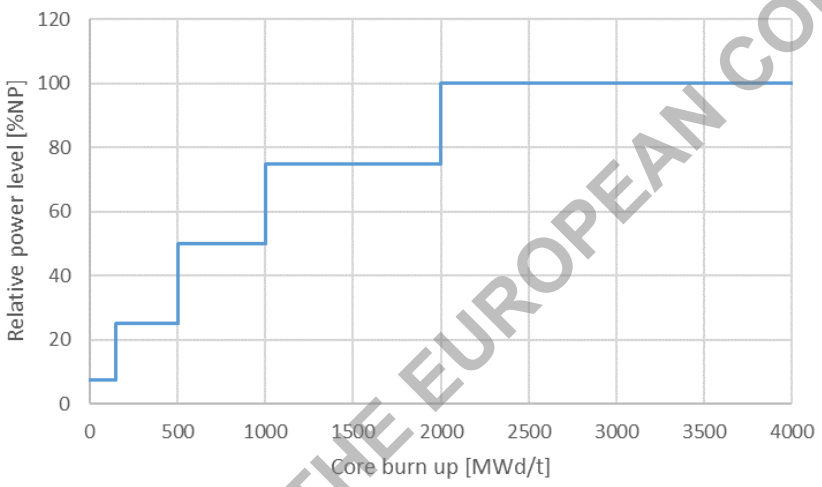

Figure 26: Start-up core power step-up

A representation of the operating temperatures diagram is shown in figure 27.

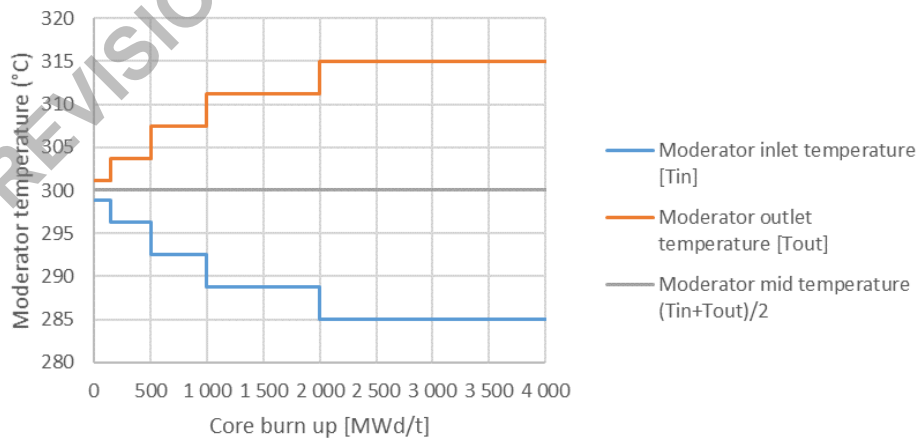

Figure 27: Operating temperatures diagram during the power step-up of the start-up core

9.Conclusion

PRATIC is a soluble boron free (SBF) small modular reactor (SMR) core of pressurized water reactor (PWR) type. Designed by the CEA (Vuiart, Eustache, Eveillard, & Prulhière, 2024), it is based on open data resources, and is distributed under creative commons licence (BY-NC-SA-4.0 licence deed, 2024). Its core was accepted to be one of the two concepts of SMR involved in the work package 7 (WP7) of the EASI-SMR European project, dedicated to providing a comprehensive characterization of boron-free cores and supporting the safety assessment of SMR cores with validated methods and industrial tools for the analysis of LW-SMR cores.

This document provides the initial data needed to model this core and to simulate its behaviour during incidental transients. While the first part gives an overview, with the PRATIC design guidelines and assumptions; the specifications of the PRATIC input data are provided in the second, with nuclear data, materials, geometries, thermal-hydraulics data and reactor management and control. All this data can be found in an updated GIT repository, access to which can be requested at the following address: pratic@cea.fr.

The first period of the WP7 will be dedicated to neutronics benchmark, in order ensure that all partners agree to the core definition and model quite the same things. Then, incidental transients will be simulated by coupling codes of several disciplines such as neutronics and thermal-hydraulics. The data provided in this document is useful for the first neutronics part.

Co-funded by the European Union
UK Research and Innovation
The Research Council of Norway
Project funded by

10. Bibliography

AREVA Design Control Document. (revision 5, September 2013). Nuclear Design. In *Final Safety Analysis Report (FSAR) of U.S. EPR* (Vols. Tier 2 / Chapter 04 - Reactor / Section 4.3, p. 7). U.S.A.: United States Nuclear Regulatory Commission (U.S. NRC). Retrieved January 2025, from https://www.nrc.gov/docs/ML1322/ML13220A678.pdf

BY-NC-SA-4.0 licence deed. (2024). Retrieved from Creative Commons: https://creativecommons.org/licenses/by-nc-sa/4.0/deed.en

Cacuci, D. G. (Ed.). (2010). *Handbook of Nuclear Engineering*. Springer. ISBN: 978-0-387-98130-7.

CEA. (2008). *Les combustibles nucléaires (Une monographie de la Direction de l'énergie nucléaire)*. (e-DEN, Éd.) Le Moniteur.

Chadwick, M. B., Herman, M., Oblozinsky, P., Dunn, M. E., Danon, Y., Kahler, A. C., . . . Kawano, T. (2011). ENDF/B-VII.1 Nuclear Data for Science and Technology: Cross Sections, Covariances, Fission Product Yields and Decay Data. *Nuclear Data Sheets*, *112*(12), 2887-2996. doi:https://doi.org/10.1016/j.nds.2011.11.002

Danrong, S., Qing, L., Dong, Q., Gaojian, D., & Chang, Z. (2021). Key Technology of ACP100: Reactor Core and Safety Design. *Nuclear Power Engineering*, *42*(4), 1-5. doi:10.13832/j.jnpe.2021.04.0001

European SMR pre-Partnership Workstream 5 –Research, Development, and Innovation Roadmap. (2023, June 30). Retrieved from SNETP - The Sustainable Nuclear Energy Technology Platform: https://snetp.eu/wp-content/uploads/2023/07/European-SMR-pre-Partnership-WS5-report-and-roadmap-30-June-2023.pdf

Godfrey, A. T. (2014). *VERA Core Physics Benchmark Progression Problem Specifications*. Oak Ridge National Laboratory, Physics Integration. revision 4 (August 29, 2014): CASL-U-2012-0131-004. Retrieved December 2024, from https://corephysics.com/docs/CASL-U-2012-0131-004.pdf

Grard, H. (2014). *Physique, fonctionnement et sûreté des REP - le réacteur en production*. EDP Sciences. ISBN: 978-2-7598-0839-7.

Hagrman, D. L., & Reymann, G. A. (1979). *MATPRO-Version 11: A Handbook of materials properties for use in the analysis of light Water reactor fuel rod behavior*. Idaho Falls: Idaho National Laboratory for the US. DOE.

Harding, J. H., & Martin, D. G. (1989). A Recommendation for the Thermal Conductivity of UO2. *Journal of Nuclear Materials*(166), 223-226.

Horelik, N., Herman, B., Forget, B., & Smith, K. (2013). Benchmark for Evaluation and Validation of Reactor Simulations (BEAVRS), v1.0.1. *Int. Conf. Mathematics and Computational Methods Applied to Nuc. Sci. & Eng.* Sun Valley, Idaho.

Ingrumeau, J. J., & Cordiez, M. (2015, December 9). Flexblue® core design: optimisation of fuel poisoning for a soluble boron free core with full or half core refuelling. *EPJ Nuclear Sci. Technol.*, *1*(11). doi:https://doi.org/10.1051/epjn/e2015-50025-3

Lautard, J. J., Loubière, S., & Feudon-Magnaud, C. (1992). CRONOS: A modular computational system for neutronic core calculations. *Specialists meeting on advanced calculational methods for power reactors; Technical committee meeting and workshop on LWR core design parameters. TECDOC-678*, pp. 42-50. Cadarache (France) and Rez (Czechoslovakia), 10-14 Sep 1990: IAEA.

Lehoux, G. (2024). *Conception Neutronique d'un cœur SMR-REP de démarrage.* Master 2 intership report from ENSI Caen school: CEA Cadarache.

Lucata, P. G., Matzke, H., & Hastings, I. J. (1996). A pragmatic approach to modelling thermal conductivity of irradiated UO2 fuel: review and recommendations. *Journal of Nuclear Materials*(232), 166-180.

Pieck, D. (2013). *Optimisation de l'utilisation du gadolinium comme poison consommable dans le combustible nucléaire : Vers un REP sans bore.* Thèse de doctorat: Aix-Marseille Université. Récupéré sur https://theses.hal.science/tel-00951801v1

(2024). *Small Modular Reactor Technology Catalogue.* A Supplement to: IAEA Advanced Reactors Information System (ARIS). IAEA.

Suk, P., Chvala, O., Maldonado, G. I., & Frybort, J. (2021, January). Simulation of a NuScale core design with the CASL VERA code. *Nuclear Engineering and Design*, *371*(110956). doi:https://doi.org/10.1016/j.nucengdes.2020.110956

TECDOC 949. (June 1997). *Thermophysical properties of materials for water cooled reactors* (ISSN 1011-4289, 1st ed.). Vienna, Austria: International Atomic Energy Agency (IAEA).

(2024). *The NEA Small Modular Reactor Dashboard: Second Edition.* OECD: Nuclear Energy Agency. Retrieved from https://www.oecd-nea.org/upload/docs/application/pdf/2024-02/7671_the_nea_smr_dashboard_-_second_edition.pdf

Toumi, I., Bergeron, A., Gallo, D., Royer, E., & Caruge, D. (2000, August). FLICA-4: a three-dimensional two-phase flow computer code with advanced numerical methods for nuclear applications. *Nuclear Engineering and Design*, *200*(1-2), 139-155. doi:https://doi.org/10.1016/S0029-5493(99)00332-5

Une, K. (1986, November). Thermal Expansion of UO2-Gd2O3 Fuel Pellets. *Journal of Nuclear Science and Technology*, *23*(11), 1020-1022. doi:https://doi.org/10.1080/18811248.1986.9735090

Vuiart, R., Brovchenko, M., Taforeau, J., Jaiswal, V., & Dumonteil, E. (2022). A Versatile Methodology for Reactor Pressure Vessel Aging Assessments. *Nuclear Science and Engineering*, *196*(4), 455-477. doi:https://doi.org/10.1080/00295639.2021.1991761

Vuiart, R., Eustache, A., Eveillard, S., & Prulhière, G. (2024). PRATIC: A soluble-boron-free, pressurized water cooled, SMR core benchmark. *EPJ Nuclear Sci. Technol.*, *10*(25). doi:https://doi.org/10.1051/epjn/2024026

Xu, B. (2016, October 18-21). CNNC's ACP 100 SMR: Technique Features and Progress in China. *13th INPRO Dialogue Forum on Legal and Institutional Issues in the Global Deployment of Small Modular Reactors.* Vienna, Austria: IAEA Headquarters. Retrieved from https://nucleus.iaea.org/sites/INPRO/df13/Presentations/011_CNNC%27s%20ACP100%20SMR-Technique%20Features%20and%20Progress%20in%20China.pdf

Yu, H., Ju, H., Wang, M., Zhang, J., Qiu, S., Tian, W., & Su, G. H. (2020, December 1). Study of boron diffusion models and dilution accidents in nuclear reactor: A comprehensive review. *Annals of Nuclear Energy*, *148*(107659). doi:https://doi.org/10.1016/j.anucene.2020.107659

Co-funded by the European Union
UK Research and Innovation
The Research Council of Norway
Project funded by

11. Appendices

These appendices are used to understand how the values at hot state (and described in section 8) were obtained. These values in appendix are not necessary to simulate the PRATIC benchmark.

11.1. Materials at 20°C

11.1.1. Fuels

The theoretical fuel density at 20°C is assumed to be 10.96 g/cm^3 [(Godfrey, 2014), p. 18]. The porosity due to sintering is assumed to be 5.5 % [(Godfrey, 2014), p. 18] which gives a real density of 10.36 g/cm^3. This real density does not account for pellet dishes and chamfers, which reduce the overall fuel volume for the same pellet stack height. Therefore, for simulations using an ideal cylindrical representation of the fuel pellets, the effective pellet density must be reduced by 0.9674 %. Thus, **the final effective fuel density at 20°C is 10.257 g/cm^3** [(Godfrey, 2014), p. 18]. Isotopic densities of standard fuels at 20°C are given in table 26 below.

Table 26: Isotopic densities of standard fuels at 20°C (in atom/barn/cm)

Enrichment in U235 / Isotope	1.6%	2.5%	2.8%	3.5%	5.0%
O16	4.5756E-02	4.5761E-02	4.5762E-02	4.5766E-02	4.5774E-02
U234	2.9933E-06	4.8549E-06	5.4893E-06	6.9910E-06	1.0289E-05
U235	3.7065E-04	5.7914E-04	6.4863E-04	8.1078E-04	1.1582E-03
U236	1.6978E-06	2.6527E-06	2.9711E-06	3.7138E-06	5.3053E-06
U238	2.2503E-02	2.2294E-02	2.2224E-02	2.2061E-02	2.1713E-02

The theoretical density of gadolinium oxide at 20°C is assumed to be 7.407 g/cm^3 [(Godfrey, 2014), p. 14]. By mixing UO_2 and Gd_2O_3 with their respective proportions noted $\%_{wt}^{UO_2}$ and $\%_{wt}^{Gd_2O_3}$, knowing the densities $\rho_{20°C}^{theo,UO_2}$ =10.96 g/cm^3 and $\rho_{20°C}^{theo,Gd_2O_3}$ =7.407 g/cm^3, considering a porosity p =5.5 % and a volume reduction ratio of Vrr =0.9674 %, we are able to calculate the effective density of gadolinium-poisoned fuels at 20°C with equation 12.

$$\rho_{20°C}^{eff,Gd_2O_3} = \frac{1}{\left(\frac{\%_{wt}^{UO_2}}{\rho_{20°C}^{theo,UO_2}} + \frac{\%_{wt}^{Gd_2O_3}}{\rho_{20°C}^{theo,Gd_2O_3}}\right)} \times (1-p) \times (1-Vrr)$$

Equation 12: Determination of final effective poisoned fuel density at 20°C

Numerical application of equation 12 gives the values reported in table 27.

Table 27: Effective density of poisoned fuel

Gadolinium ratio	2%	8%
Effective density of poisoned fuel (g/cm^3)	10.1595	9.8779

Knowing that all UO_2-Gd_2O_3 fuels of PRATIC are composed of LEU enriched at 2.5% in ^{235}U, isotopic densities of gadolinium-poisoned fuel at 20°C are given in the table below.

Table 28: Isotopic densities of gadolinium-poisoned fuels at 20°C

Gd_2O_3 mass ratio / Isotope	2.0%	8.0%
Gd152	1.3503E-06	5.2513E-06
Gd154	1.4718E-05	5.7239E-05
Gd155	9.9919E-05	3.8860E-04
Gd156	1.3820E-04	5.3747E-04
Gd157	1.0566E-04	4.1091E-04
Gd158	1.6770E-04	6.5221E-04
Gd160	1.4758E-04	5.7397E-04
O16	4.5432E-02	4.4482E-02
U234	4.7126E-06	4.3015E-06
U235	5.6216E-04	5.1311E-04
U236	2.5750E-06	2.3503E-06
U238	2.1640E-02	1.9752E-02

11.1.2. Cladding material

The fuel cladding material is composed of Zircaloy-4 material (Zy4). The element composition is taken from (Horelik, Herman, Forget, & Smith, 2013), page 144 of the revision 3.0 of this document (dating from 14 July 2020). This composition is shown in table 29. The density of this material is assumed to be 6.55 g/cm^3 at 20 °C [(Horelik, Herman, Forget, & Smith, 2013), pp. 50 and 144 of the revision 3.0 of this document, dated from July, 14th 2020].

Table 29: Elemental composition of Zircaloy-4

Element	Weight fraction
Zr	98.115%
Sn	1.45%
Fe	0.21%
O	0.125%
Cr	0.10%

11.1.3. Structural material

AISI 304 (also named SS-304) is a grade of austenitic stainless steel that is used in PRATIC in reflectors, in neutron absorber cladding and in some absorber rods that compose grey control rods. Its element composition is taken from [(Horelik, Herman, Forget, & Smith, 2013), p. 143 of

the revision 3.0 of this document dating from 14 July 2020] and reported in table 30. The density of this material is assumed to be 8.03 g/cm^3 at 300 K, which corresponds to 27 °C.

Table 30: Elemental composition of AISI 304

Element	Weight fraction
Fe	68.4%
Cr	19.0%
Ni	10.0%
Mn	2.0%
Si	0.6%

11.1.4. Absorber materials

Materials used in absorber rods are silver-indium-cadmium alloy (also named AgInCd or AIC) or Stainless Steel 304 alloy (also called SS-304). For this later one, its description is given in the section 11.1.3 Structural material.

The composition of AIC is given in table 31 and taken from [(Godfrey, 2014), p. 10] or [(Horelik, Herman, Forget, & Smith, 2013), p. 139 of the revision 3.0 of this document]. The density of AgInCd is assumed to be 10.17 g/cm^3 at 20°C and is taken from [(TECDOC 949, June 1997), p. 128].

Table 31: Elemental composition of AIC

Element	Weight fraction
Ag	80%
In	15%
Cd	5%

Co-funded by the European Union
UK Research and Innovation
The Research Council of Norway
Project funded by

11.2. Geometries at 20°C

All the geometric values are taken from (Godfrey, 2014). These values at 20 °C are given in table 32.

Table 32: Dimensions at 20 °C

Element	Value at 20 °C	Unit	Filling material
Fuel pellet radius	0.4096	cm	UO_2 or $UO_2Gd_2O_3$
Inner fuel clad radius	0.4180	cm	He
Outer fuel clad radius	0.4750	cm	Zy4
Inner guide tube radius	0.5610	cm	H_2O
Outer guide tube radius	0.6020	cm	Zy4
Inner instrument tube radius	0.5590	cm	H_2O
Outer instrument tube radius	0.6050	cm	Zy4
AIC rod radius	0.3820	cm	AIC
SS-304 rod radius	0.3820	cm	SS-304
Inner absorber cladding radius	0.3860	cm	He
Outer absorber cladding radius	0.4840	cm	SS-304
Cell pitch	1.2600	cm	H_2O
Assembly pitch	21.5000	cm	-
Inter-assembly half gap	0.0400	cm	H_2O
Core active height	200.0000	cm	-

11.3. Thermal expansion laws and material densities

The linear thermal expansion laws used to translate dimensions or densities from cold to hot state are written in equations 13 to 17 below.

For silver-indium-cadmium (AgInCd or AIC) absorbents, the expansion coefficient is calculated with equation 13 [adapted from reference (TECDOC 949, June 1997), p. 129], with a reference temperature of 27°C (corresponding to 300 K) and T is the temperature of the medium expressed in Celsius degrees.

$$\frac{L+\Delta L}{L} = 1 + \left(2.25 \times 10^{-5} \times (T - 27)\right)$$

Equation 13: Linear thermal expansion law of AgInCd

For Stainless Steel 304 (SS-304), the expansion coefficient is calculated with equation 14 [adapted from reference (TECDOC 949, June 1997), p. 133], with a reference temperature of 27°C (corresponding to 300 K) and T is the temperature of the medium expressed in Celsius degrees.

$$\epsilon(T) = 1.57 \times 10^{-5} \times (T + 273) + 1.69 \times 10^{-9} \times (T + 273)^2$$
$$\frac{L+\Delta L}{L} = 1 + \epsilon(T) - \epsilon(27)$$

Equation 14: Linear thermal expansion law of SS-304

For uranium dioxide UO_2, the expansion coefficient is calculated with equation 15 [adapted from reference (TECDOC 949, June 1997), p. 40, law issued from "MATPRO"], with a reference temperature of 27°C (corresponding to 300 K) and T is the temperature of the medium expressed in Celsius degrees.

$$\frac{L+\Delta L}{L} = 1 + \left(-3.0\times10^{-3} + 1.0\times10^{-5}\times(T+273) + 4.0\times10^{-2}\times\exp\left(\frac{-6.9\times10^{-20}}{k_B(T+273)}\right)\right)$$

Equation 15: Linear thermal expansion law of UO_2

For gadolinium poisoned uranium oxide (UO_2-Gd_2O_3), the expansion coefficient is calculated with equation 16 [adapted from reference (Une, 1986), table 1 with 8 %wt. of gadolinium content], with a reference temperature of 22°C (corresponding to 295 K[4]) and T is the temperature of the medium expressed in Celsius degrees.

$$\frac{L+\Delta L}{L} = 1 + (-2.391\times10^{-3} + 7.433\times10^{-6}\times(T+273) + 2.278\times10^{-9}\times(T+273)^2)$$

Equation 16: Linear thermal expansion law of UO_2-Gd_2O_3

For Zircaloy-4 (Zr4), the expansion coefficient is calculated with equation 17 [adapted from reference (TECDOC 949, June 1997), p. 70], with a reference temperature of 20°C (corresponding to 293 K) and T is the temperature of the medium expressed in Celsius degrees.

$$\frac{L+\Delta L}{L} = 1 + \left(5.2\times10^{-6}\times(T-20)\right)$$

Equation 17: Linear thermal expansion law of Zr4

Numerical applications of equations 13 to 17 for several temperatures T are reported in table 33.

Table 33: Linear thermal expansion coefficients with various reference temperatures

	(L+ΔL)/L from reference temperature in bold to XX°C					
Material	20	22	27	285	300	315
AgInCd	0.999843	0.999955	1	1.005805	1.006143	1.006480
SS-304	0.999883	0.999967	1	1.004425	1.004689	1.004954
UO_2	0.999930	0.999980	1	1.002585	1.002737	1.002888
UO_2-Gd_2O_3	0.999982	1	1.000044	1.002466	1.002616	1.002767
Zircaloy-4	1	1.000026	1.000036	1.001378	1.001456	1.001534

These coefficients are adapted to all have the same reference temperature of 20°C, and the values are reported in table 34.

[4] Contrary to what is written in (Une, 1986), the reference temperature for the coefficient of UO_2-Gd_2O_3 is 295 K

Co-funded by the European Union
UK Research and Innovation
The Research Council of Norway
Project funded by

Table 34: Linear thermal expansion coefficients with a unique reference temperature of 20°C

	(L+ΔL)/L from reference temperature in bold to XX°C					
Material	20	22	27	285	300	315
AgInCd	1.000000	1.000113	1.000158	1.005963	1.006301	1.006639
SS-304	1.000000	1.000084	1.000117	1.004542	1.004806	1.005071
UO_2	1.000000	1.000050	1.000070	1.002655	1.002807	1.002958
UO_2-Gd_2O_3	1.000000	1.000018	1.000061	1.002484	1.002634	1.002785
Zircaloy-4	1.000000	1.000026	1.000036	1.001378	1.001456	1.001534

Thanks to these coefficients, the values of density for each material of interest are calculated for several temperatures in table 35. For each material, one value is written in bold and italic: this is the reference density of the material at the chosen reference temperature. For UO_2 and UO_2-Gd_2O_3, the reference was arbitrary chosen at 20°C.

Table 35: Densities of materials at several temperatures

	Density (g/cm³) at XX°C					
Material	20	22	27	285	300	315
AgInCd	10.1748	10.1714	***10.17***	9.9949	9.9849	9.9748
SS-304	8.0328	8.0308	***8.03***	7.9243	7.9181	7.9118
UO_2	***10.2570***	10.2554	10.2548	10.1757	10.1711	10.1665
UO_2-8%Gd_2O_3	***9.8779***	9.8774	9.8761	9.8047	9.8003	9.7959
UO_2-2%Gd_2O_3	***10.1595***	10.1590	10.1577	10.0842	10.0797	10.0751
Zircaloy-4	***6.55***	6.5495	6.5493	6.5230	6.5215	6.5199

The geometry is expanded axially and radially following these assumptions:

- The expansion of the active zone height is driven by the fuel (UO_2) coefficient at 300 °C. As the expansion coefficient of Zy4 is lower than this of UO_2, this implies a slight gain in the number of atom of Zy4 in the active zone (neutron effect is assumed to be negligible).
- All the elements of the active zone (cladding, guide tubes, assembly pitch, etc.) are expanded in the 3 directions at 300 °C and the water fills the free volume outside the fuel pins.
- The densities of materials that compose the reflectors are expanded at 300 °C, but the height of the axial reflectors still remain 20 cm. Nevertheless, the reflectors "radial pitch" is expanded at 300 °C like the radial assembly pitch.
- The absorber rods are assumed to be expanded axially and radially, with the corresponding density of the materials at 300 °C filling the volumes, but the management of the "zero level" of the control rods (see section 8.3.4.4 page 28) erases the effect of the axial expansion.

EASI SMR